Optic flow in human vision: MEG reveals a foveo-fugal bias in V1, specialization for spiral space in hMSTs, and global motion sensitivity in the IPS

Ian E. Holliday

School of Life and Health Sciences, Aston University, Birmingham, UK

Timothy S. Meese

School of Life and Health Sciences, Aston University, Birmingham, UK

We recorded MEG responses from 17 participants viewing random-dot patterns simulating global optic flow components (expansion, contraction, rotation, deformation, and translation) and a random motion control condition. Theta-band (3–7 Hz), MEG signal power was greater for expansion than the other optic flow components in a region concentrated along the calcarine sulcus, indicating an ecologically valid, foveo-fugal bias for unidirectional motion sensors in V1. When the responses to the optic flow components were combined, a decrease in MEG beta-band (17–23 Hz) power was found in regions extending beyond the calcarine sulcus to the posterior parietal lobe (inferior to IPS), indicating the importance of structured motion in this region. However, only one cortical area, within or near the V5/hMT+ complex, responded to all three spiral-space components (expansion, contraction, and rotation) and showed no selectivity for global translation or deformation: we term this area hMSTs. This is the first demonstration of an exclusive region for spiral space in the human brain and suggests a functional role better suited to preliminary analysis of ego-motion than surface pose, which would involve deformation. We also observed that the rotation condition activated the cerebellum, suggesting its involvement in visually mediated control of postural adjustment.

Keywords: human vision, complex motion, V5, MT, MST, intraparietal sulcus, radial motion, optic flow, MEG, hMSTs

Citation: Holliday, I. E., & Meese, T. S. (2008). Optic flow in human vision: MEG reveals a foveo-fugal bias in V1, specialization for spiral space in hMSTs, and global motion sensitivity in the IPS. *Journal of Vision, 8*(10):17, 1–24, http://journalofvision.org/8/10/17/, doi:10.1167/8.10.17.

Introduction

Visual mechanisms for optic flow

The array of complex retinal motions that occur as an observer moves through a structured environment is referred to as optic flow. Within certain constraints, this flow can be decomposed mathematically into three pairs (six cardinal axes) of orthogonal vector fields. These are expansion/contraction and rotation, sometimes referred to as spiral space (Graziano, Andersen, & Snowden, 1994; Heuer & Britten, 2007; Meese & Anderson, 2002; Morrone, Burr, Di Pietro, & Stefanelli, 1999; Snowden & Milne, 1996), two components of deformation (deformation space), and two components of translation (translation space; Koenderink, 1986; Koenderink & van Doorn, 1975; Longuet-Higgins & Prazdny, 1980). A point within translation space represents a single direction of uniform motion, whereas points in spiral and deformation spaces represent uniform distributions of all local directions (i.e., the motion is two-dimensional in the plane). These two-dimensional motions are sometimes referred to as complex motions (see Figure 1 for iconic examples).

Optic flow provides the observer with useful information such as direction of heading (Gibson, 1950; Lappe, Bremmer, & van den Berg, 1999; Warren & Hannon, 1988), time to contact (Lee, 1980), distance traveled (Redlick, Jenkin, & Harris, 2001), segmentation of object motion (Logan & Duffy, 2006; Warren & Rushton, 2008), and the slant and tilt (pose) of surfaces in the scene (Koenderink, 1986). And there is good evidence that the human visual system takes advantage of some of these. For example, observers can identify the focus of expansion (Bex & Falkenberg, 2006; Warren, Morris, & Kalish, 1988) and make accurate judgements of their heading based on this (Crowell & Banks, 1993), even in the presence of head and eye movements (Royden, Banks, & Crowell, 1992; Royden & Picone, 2007). A large-scale (global) analysis of the expansion component in optic flow is used to judge time-to-contact (Giachritsis & Harris, 2005), rotation is used to compensate retinal flow for observer roll (Hanada & Ejima, 2000), expansion and rotation influence posture (Lee & Aronson, 1974;

doi: 10.1167/8.10.17 Received June 20, 2008; published December 30, 2008 ISSN 1534-7362

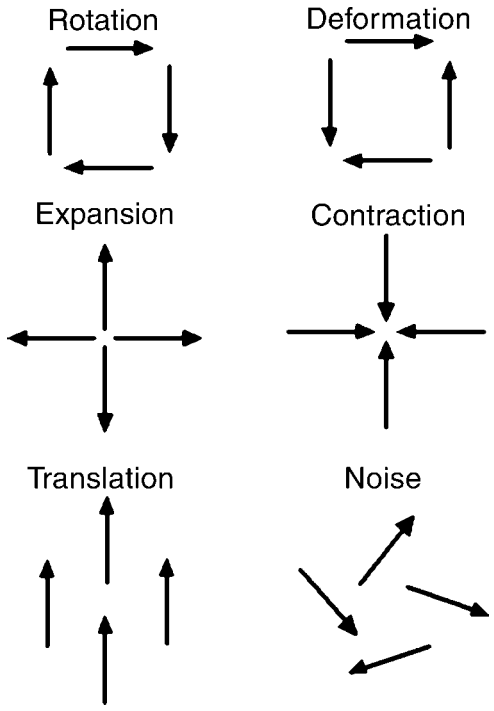

Figure 1. Iconic illustrations of the transformations applied to the dot motions used in the various experimental conditions. In the stimuli used in the experiments dot directions were evenly distributed around all directions for all stimulus conditions, with the exception of translation, which always moved upward. Stimuli changed smoothly from a control condition (random directions, bottom right) to one of the other five conditions over a period of 364 ms. Subsequent changes back to random motion were carried out in the same way.

Richards, Mulavara, & Bloomberg, 2004), and deforming random-dot displays give a profound sense of moving surfaces with distinct slant and tilt (Domini & Caudek, 1999; Freeman, Harris, & Meese, 1996; Meese & Harris, 1997; Meese, Harris, & Freeman, 1995; Zhong, Cornilleau-Pérès, Cheong, Yeow, & Droulez, 2006). Thus, there is a clear functional distinction between spiral space, which provides information about the observer's position within, and relation to the environment (ego-motion), and deformation space, which provides information about the environment's layout and structure.

Evidence that primate vision contains the appropriate specialized mechanisms to perform these analyses comes from psychophysics (Bex, Metha, & Makous, 1998, 1999; Burr & Santoro, 2001; Freeman & Harris, 1992; Gurney & Wright, 1996; Meese & Harris, 2001a, 2001b; Morrone, Burr, & Vaina, 1995; Snowden & Milne, 1996, 1997), single-cell recordings (Duffy & Wurtz, 1991a, 1991b; Saito et al., 1986; Tanaka & Saito, 1989), and functional imaging (Dupont, Orban, De Bruyn, Verbruggen, & Mortelmans, 1994; Goossens, Dukelow, Menon, Vilis, & van den Berg, 2006; Morrone et al., 2000; Smith, Wall, Williams, & Singh, 2006). In principle, the entire optic flow (the six dimensions described above) could be encoded by twelve elementary mechanisms, assuming that opposite sign (e.g., clockwise and anticlockwise rotation) is carried by different mechanisms. This requires that the mechanisms have broad tuning, largely consistent with psychophysical observations (Meese & Anderson, 2002; Meese & Harris, 2001a). There is also evidence that optic flow can be decomposed into its component parts (Barraza & Grzywacz, 2005), but it seems unlikely that this is done at the single-cell level (Barraza & Grzywacz, 2005) and that intermediate mechanisms along the cardinal dimensions are probably also involved (Graziano et al., 1994; Meese & Anderson, 2002; Snowden & Milne, 1996) as well as combinations across the three vector fields (Duffy & Wurtz, 1997a).

Anatomical loci of the optic flow mechanisms

Evidence is accumulating of an extensive network of motion sensitive regions in the parietally directed stream of visual cortex, both within and beyond the well-established V5/MT cortical area (Annese, Gazzaniga, & Toga, 2005; Dumoulin et al., 2000; Van Essen, Maunsell, & Bixby, 1981). The cortex in the proximity of the classically defined V5/MT area (including MST) is subdivided into several modules supporting different aspects of motion analysis (Huk, Dougherty, & Heeger, 2002; Matsumoto et al., 2004), and many authors now refer to this region as the MT+ or MT complex to reflect this fact. In this paper we also use the term hMT+ to identify the human cortical area homologous to the region identified in monkeys as MT+ (Beauchamp, Cox, & DeYoe, 1997). In addition to the MT complex there are many reports of motion processing outside this region. The posterior zone of the intraparietal sulcus (IPS) and the inferior parietal lobule in particular have been observed to support higher order motion processing (Claeys, Lindsey, De Schutter, & Orban, 2003; Martinez-Trujillo, Cheyne, Gaetz, Simine, & Tsotsos, 2007; Orban et al., 2006).

Antecedents to the present work

In a previous experiment (Holliday & Meese, 2005) using abrupt onsets of motion stimuli we obtained clear evoked responses to several types of optic flow components. The evoked responses were largest for the expansion (radiating) component, with marginally smaller amplitudes for contracting and rotating patterns. Other studies have also found biases for outward radiation (Beardsley & Vaina, 2005; Gilmore, Hou, Pettet, & Norcia, 2007; Ptito, Kupers, Faubert, & Gjedde, 2001). Biases for inward radiation have been found too (Edwards & Badcock, 1993; Giaschi, Zwicker, Young, & Bjornson, 2007), though universal support for this result has not

been found psychophysically (Meese & Anderson, 2002; Morrone et al., 1999; Snowden & Milne, 1996; see Holliday & Meese, 2005 for further information).

Applying MEG dipole source localization methods (Baillet et al., 2001; Barth, Sutherling, Broffman, & Beatty, 1986; Cohen, 1972; Crouzeix, Yvert, Bertrand, & Pernier, 1999) to the analysis of the evoked responses in our previous study gave results often dominated by a single source solution in or close to the inter-hemispheric fissure (unpublished observation). However, a more likely interpretation is that this result arose from summation of symmetric sources either side of the midline. Therefore, additional evidence was sought in the present study to identify the cortical regions involved.

An alternative to single equivalent dipole analysis to identify the sources of MEG activations is to apply one of a range of source reconstruction methods (Hillebrand & Barnes, 2005; Hillebrand, Singh, Holliday, Furlong, & Barnes, 2005; Jensen & Vanni, 2002; Liljeström, Kujala, Jensen, & Salmelin, 2005; Vrba & Robinson, 2001). Using synthetic aperture magnetometry (SAM—see Methods section) applied to our pilot data (Holliday & Meese, 2001) suggested that extra-striate effects were strongest when images were obtained for cortical oscillation frequencies within the beta frequency band (nominally 15–25 Hz) and localized in regions around the posterior part of the parietal lobe in the region of the IPS.

Stimulus onset design

Because evoked responses arise from phase-locking to the stimulus, these are more likely to reflect linked activation in earlier stages of the perceptual process. Further on in the perceptual process, phase-locking to the stimulus onset is likely to be weaker and thus induced responses are likely to dominate the experimental effects. Motion onset has been demonstrated to produce strong bursts of action potentials in primary visual cortex and in MT+ in primates (Cook & Maunsell, 2002; Orban et al., 2003; Orban, Van Essen, & Vanduffel, 2004), and it seems likely that summation of the associated phase-locked local field potentials underlies several components of the evoked response obtained with motion onset stimulation. Therefore to optimize our stimuli to activate extra-striate regions and eliminate or, at least diminish, the dominance of evoked responses to broadband stimulus transients, we used an experimental paradigm in which sharp motion onsets were removed. We did this by using limited lifetime, random-dot displays, where structured motions emerged smoothly from random noise patterns that contained dot velocities matched to those in the structured test stimuli. Thus, the distributions of local motion speeds and dot densities were (approximately) constant throughout the recording period, any fluctuations having no correlation with the onset of motion coherence. With this design our experiments were more likely to reveal brain activity that does not depend on phase-locked (onset-driven) signals, but intrinsic properties of the cortical motion processes.

Choice of optic flow components

In addition to the random-dot control pattern we used several optic flow components as test stimuli. As outlined above there are six dimensions of optic flow, suggesting a total of twelve different elementary stimulus conditions (six dimensions, times two signs). However, for the purposes of experimentation, this can be reduced considerably. A rotation of the polar coordinate in translation space simply transforms the direction of uniform motion. Although oblique motion effects are known (e.g., Dakin, Mareschal, & Bex, 2005; Greenwood & Edwards, 2007), they are not of particular interest here, so we chose a single direction of translation. Direction discrimination thresholds and natural movie statistics are very similar for upward, leftward, and rightward motions (Dakin et al., 2005). However, we judged that motion in the vertical meridian was less likely to induce eye movements than that in the horizontal meridian, so we chose to study translating motion that moved upward.

It is also the case that rotating the polar coordinate in deformation space results in a global rotation of the deformation vector field without changing the structure of the pattern. Therefore we chose to investigate only a single component of deformation. The one we chose (its sign was arbitrary) was consistent with that carried by a planar surface with the same tilt as the ground and ceiling plane (e.g., it contained a component of horizontal shear; see Figure 1). These surfaces are presumably more common than those with orthogonal tilt (e.g., walls and doors).

Spiral space has a different property from the other two spaces. A rotation of polar angle in this space changes the structure of the complex motion: from expansion to clockwise rotation, through contraction to anticlockwise rotation. While there is no reason to suppose different functional significances for the two directions of rotation, this is not so for expansion/contraction. This is because locomotion is typically forwards (not backwards), and this produces an expanding (outward radiating) optic flow field. Therefore, we chose to investigate three components from this space: expansion, contraction and (clockwise) rotation. This gave five coherent motion (optic flow) patterns in total: translation plus four complex motions (see Figure 1). This is a more complete set of optic flow stimuli than has been used in previous imaging studies (e.g., Huk et al., 2002; Morrone et al., 2000; Smith et al., 2006; Wall, Lingnau, Ashida, & Smith, 2008; Wall & Smith, 2008).

Our main strategy was to compare the MEG responses to each of the five test conditions against random motion, with the aim of identifying the brain regions involved in

processing these coherent global motions. However, to help validate comparisons across these conditions we required that they all had the same distribution of local dot speeds. To do this we removed the speed gradients from the complex motion components, but left their direction templates intact. The speeds of the complex motions were then matched to that of the translation stimulus (e.g., Morrone et al., 2000).

Aims

Our main aims were three-fold:

1. To determine the oscillatory frequency bands in the cortex most strongly associated with the processing of optic flow components.
2. To clarify the regional distribution of these responses across the cortex, with a view to further investigating the involvement of the dorsal steam with optic flow.
3. To examine the relative strengths of responses to the different motion patterns.

This was to identify the location or locations of the expansion bias (Holliday & Meese, 2005), and to characterize the selectivity of individual cortical motion modules to better understand their functional roles.

Overview

There are four parts to our analysis. In Part 1 we analyze the evoked MEG response averaged across sensors. This provides a detailed account of the morphology of the neuro-magnetic waveforms and demonstrates the success of our stimulus design: the evoked effects were too small to reveal stimulus-specific responses in our data set and unlikely to have masked the induced effects upon which we focus. That we were able to find an evoked response at all (only after widespread averaging) was something of a surprise. The reader who is concerned less with the technical details of the evoked response and more with our functional findings regarding the specific brain regions involved with optic flow could skip over these first parts of the results and discussion without loss of continuity. In Part 2 we use a very different approach; we analyze the data using synthetic aperture magnetometry (SAM) in the theta band: a frequency band that might 'pick up' the weak evoked response among other effects. In general, our SAM analysis delivered data sets for which stimulus-specific effects were readily seen. For example, in the theta band we see a clear expansion bias in V1, confirmed by conventional statistical analysis. In Part 3 we extend our SAM analysis to the higher frequency, beta band. We found:

1. a brain region specialized for spiral space (hMSTs),
2. the involvement of structured motion in a substantial occipito-parietal region inferior to the IPS, and
3. a rotation specific effect in the cerebellum.

In a short Part 4, we report the absence of any further effects in the alpha and gamma bands.

Methods

Participants

The experiment was performed with the help of 17 adult volunteer participants. All had previous experience of MEG participation, and a recent anatomical MRI image of the head available to use in the analysis. Stimuli were viewed binocularly and participants used their normal contact lens optical correction if required. Participants gave their informed consent prior to the experiment. Ethical permission for the experimental procedure was provided by the Aston University Human Sciences Ethical Committee.

Stimuli

Stimuli were generated on a Cambridge Research Systems VSG 2/3 graphics system back-projected onto a translucent screen at a viewing distance of approx. 25.5 cm. They comprised 200 randomly positioned white dots moving within a circular field approximately 76 deg in diameter, giving a dot density of ~1 dot per 23 deg^2 (a very similar density to that used by Morrone et al., 2000). Dot contrast was ramped to zero over a few degrees around the perimeter to avoid sharp transients as dots transited the edge. Each dot moved along a straight trajectory for 364 ms (their 'finite-lifetime') with a speed of 6.2 deg/s over ten movie frames and was then replotted at a new random position and subsequently moved along a trajectory computed in accordance with one of the types of motion employed in the experiment. In a control condition, these trajectories had random directions. In the test conditions they depicted one of five types of structured motions. These were closely related to elementary components of the optic flow field (Koenderink & van Doorn, 1975; Longuet-Higgins & Prazdny, 1980): expansion, contraction, rotation, deformation (all with spatial speed gradients removed), and planar translation upward (see Figure 1). The construction of our stimuli ensured that the average dot densities and dot speeds were constant for the entire recording period.

Test and random (control) stimuli alternated with durations of 1.82 s and 3.64 s, respectively, and the linear transition period between maximum signal coherence (90%) and 100% noise was 364 ms (total epoch duration was 5.45 s). The five different structured motions were

presented 40 times randomized in a single block of 200 trials and observers were instructed to fixate a central stationary point throughout the experiment. A few additional catch trials were incorporated that participants were instructed to attend for and count. These were identical to a normal stimulus presentation except that the brightness of the display dots was reduced to half its usual value, producing a marked reduction in stimulus contrast. At the conclusion of the block, participants reported the number of catch trials and their performance was fed back to them. Sections of the data containing a catch trial were discarded. No other data were excluded.

Note that static frames of our displays were quite sparse; on average they contained only one dot for every unit square with a side of 4.8 deg (about 2 cm on the screen). However, over the test-signal duration of 1.82 sec, each unit square contained an average of five independently placed dots, each of which traveled a distance of 2.3 deg. This produced 'busy' looking stimuli with good coverage of the display region.

MEG recordings

MEG signals were acquired using a 151-channel whole-head CTF Omega System (VSM MedTech, Vancouver, Canada) within a magnetically shielded environment (1-layer mu-metal alloy and 1-layer aluminum room manufactured by Vacuumschmeltze, Germany) at 625 Hz sampling rate. Hardware filter setting were 0 Hz–208.3 Hz. The MEG system incorporated several reference sensor array used for environmental noise suppression, and the subsequent analysis used a third-order software gradiometer that produced a sensitivity of about 10 $fT/Hz^{1/2}$ above 0.1 Hz (Vrba & Robinson, 2001). Data were collected in "epochs" of 3.0 s from the period 1.0 s prior to the first frame on which a coherent motion stimulus appeared, to 2.0 s after this time. Data collection was synchronized to the appearance of the stimuli by using a photodiode placed on the projection screen such that it received the light from a small white square (obscured from the participants' view) that appeared at the stimulus onset time. This was needed as the LCD projector technology we used did not permit accurate control of the projection timing in relation to the timing of video streamed from the graphics computer. In this way, data segments for analysis were selected with respect to the time of display onset indicated by the photodiode pulse. The recorded data were post-processed to remove baseline offset levels by subtracting the mean recorded magnetic field value for the 1.0 s pre-onset period from the whole epoch. A 50-Hz comb filter was applied to suppress environmental noise from remote electrical sources. Low- and high-pass filters (4th-order Butterworth) were also applied with a low-pass 10-dB roll-off point of 70 Hz and high-pass roll-off at 0 Hz for the theta range analysis and 2 Hz for the other frequency bands of interest.

Participants were fitted with three small solenoid coils placed near the nasion, and the left and right pre-auricular notches. The positions of the reference coils were first used to digitize the shape of the participants' heads using a Polhemus IsoTrak system. The digitized head shapes were subsequently used to co-register the MEG data with the participants' MRIs (obtained elsewhere on different occasions on various MRI systems); these provided the framework for the anatomical interpretation of the results (Adjamian et al., 2004). The coils remained in position on the participants' heads during the experiments; alternating current was passed through the coils allowing the position of the coils to be determined by the MEG acquisition system immediately before and after the recording sessions. This localization information is used to establish the spatial relationships between the participants' heads and the MEG sensor array.

MEG analysis methods

The results of the experiment were analyzed using evoked response averaging and Synthetic Aperture Magnetometry (SAM; Vrba & Robinson, 2001). SAM is an adaptive spatial filtering algorithm or 'beamformer'. The beamformer is a linear combination of the signals recorded on all the sensors, optimized such that the signal estimated at a point is unattenuated while remote correlated interfering sources are suppressed. The technical details and a discussion of the limitations of the SAM method are described in Hillebrand and Barnes (2005). SAM is applied to frequency band-limited samples of the data and is used here to provide a statistical measure of the difference in power in the comparison of two sets of data samples as a pseudo-T value [*pseudo-T* values arise as the estimate of the random error term in the t-test is taken as the variance of the lowest component in a singular value decomposition of the data covariance matrix]. Data samples are selected for specified time periods with respect to the stimulus onset time, thus a contrast can be made between the pre- and post-stimulus onset periods for a given stimulus condition, or over the same time window in the post-stimulus period for two experimental conditions. SAM analysis was applied in our analysis on a $5 \times 5 \times 5$ mm grid of points throughout the brain volume, producing at each grid point an estimate of the statistical significance of differences in response magnitude as a pseudo-T value. SAM analysis was conducted in the following frequency bands: 3–7 Hz (nominally 'theta'), 8–13 Hz (nominally 'alpha'), 17–23 Hz (nominally 'beta'), and 30–75 Hz (nominally 'gamma'). Additional analysis of group effects was performed using statistical parametric mapping methods with the matlab statistical parametric mapping packages SPM99 and SPM2, and the non-parametric package SnPM (Singh, Barnes, & Hillebrand, 2003). Using these methods individual results were transformed into a standard

anatomical framework (using the MNI152 T1 template supplied in SPM packages) to provide an analysis at the group level (http://www.fil.ion.ucl.ac.uk/spm/). SnPM (http://www.sph.umich.edu/ni-stat/SnPM/) is a non-parametric method that estimates the statistical distribution of the data under the null hypothesis. The observed values are then compared against the estimated null distribution to assign probabilities of observation under the null hypothesis ('p-values') to the results. A good introduction to this method is provided by Nichols and Holmes (2001). Results from the statistical parametric mapping analysis of the grouped data were visualized using mri3dx (http://www.aston.ac.uk/lhs/research/groups/nrg/mri3dx/). Sites and volumes of significant activation were reported by the SPM software in MNI coordinates. Therefore to produce coordinates for reference to the Talairach and Tournoux (1988) brain atlas we transformed these using the icbm_spm2tal coordinate transformation (Lancaster et al., 2007) supplied with Java program gingerALE available from http://www.brainmap.org/index.html. These coordinates were then referred to the Talairach Daemon Java program (http://ric.uthscsa.edu/projects/talairachdaemon.html) to identify corresponding brain regions.

Averaged evoked responses were also calculated for each participant, in each condition; the filtering and preprocessing parameters applied were as described above. Averaged responses of individual participants were examined as were the results after combining data sets for all the participants in each condition and finally after combining the results across all participants and conditions. No correction was made for relative spatial alignment differences between the sensor arrays when combing data sets across participants for evoked response analysis.

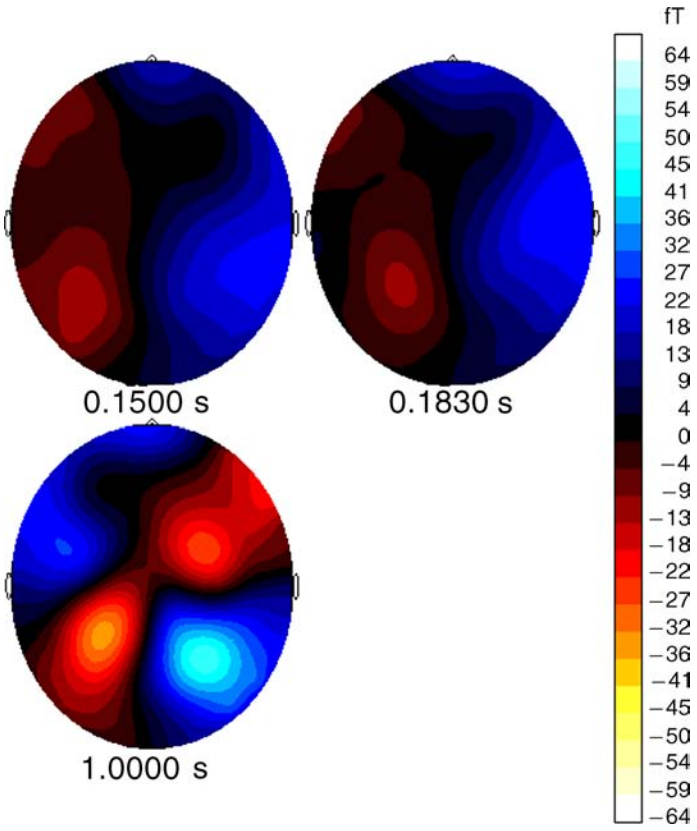

Figure 2. Averaged evoked magnetic field plotted over the sensor array at three times (*t*) relative to the onset of motion coherence. Average values were for all conditions and participants. Top left panel: *t* = 150 ms. Top right panel: *t* = 183 ms. Lower left panel: *t* = 1000 ms. Anterior/posterior is shown top/bottom; Left/right is shown left/right.

Results

Part 1. MEG evoked responses

The application of signal averaging in individual participants produced no evidence of evoked responses on a visual inspection of the averages for any condition in any participant. This was anticipated as the stimulus design was such that abrupt onsets of stimulus contrast or stimulus motion were avoided. Averages were also made by combining participant data for each condition and finally by combining all data for each participant and condition. Again there was little evidence of average evoked responses when data were combined over conditions but, surprisingly, in the case of combining the data over all conditions and participants there was some evidence of average evoked response effects.

We observed two phenomena in the averaged data. The first of these was a very small evoked response with a typical morphology, first being distinguishable from the background level at about 150-ms post-coherence onset rising to a peak at about 183 ms. The magnitude of the response was very small with maximum amplitude of some 10–20 fT/Hz$^{1/2}$, which was close to the sensor noise level. This response is evident in a plot of the magnetic field distribution over the sensor array shown in Figure 2 (top) at latencies of 150-ms and 183-ms post-coherence onset. The field map is consistent with at least one source near the midline in the occipito-parietal region, but as the data were derived from pooling over multiple conditions and participants, we did not pursue this analysis further.

A more remarkable observation is that there was a slowly increasing static DC field that accumulated over a period approximately from 0.5 s after the onset of coherent motion to the end of the recording period 1.5 s later. The field map at 1-s post-stimulus onset is consistent with at least two sources, bilaterally symmetrically placed about the midline in the parieto-occipital regions (Figure 2, bottom left). Figure 3 shows the response time series from each sensor overlaid with a colored bar added to identify the period 0.0–0.5 s. Note that the early evoked response (within the colored bar) is hardly noticeable compared to the main DC effect (beyond the colored bar).

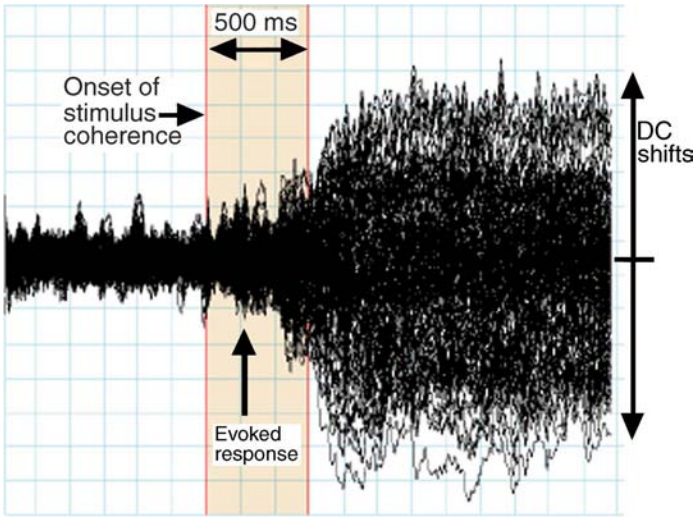

Figure 3. Overlay of all sensor data filtered into the band 0–40 Hz and averaged over stimulus types and participants for the period −1.0 s to 2.0 s relative to the onset of motion coherence. The beige bar extends from t = 0.0 s to 0.5 s. Note that the DC shifts start about 500 ms after the onset of stimulus coherence. Each square is a period of 167 ms and an amplitude of 10 fT/sqrt(Hz).

The effects are more easily discerned in Figure 4, which shows the averaged sensor time series picked off for four of the sensors above the right parietal lobe (selected to illustrate the typical morphology of the waveforms). The early evoked response is just visible. It had a peak amplitude at about 183 ms, a duration of about 150 ms, and a nominal frequency of about 3.3 Hz (we estimated this from the biphasic form of the evoked response over a period of about 1/3 s).

The DC field was of much larger amplitude reaching a maximum value after about 1 s and had a positive sign in each of these four examples. These correspond to curves in the upper part of the data cloud in Figure 3 and sensors in the blue regions in Figure 2. Similar curves with approximately reversed morphology occurred for sensors in the complementary parts of the magnetic field (lower cloud in Figure 3 and red in Figure 2).

Part 2. SAM analysis: Theta (3–7 Hz)

The expansion bias is in V1

Figure 5 shows the results of a SAM group analysis of data from 17 participants for comparisons of the expansion

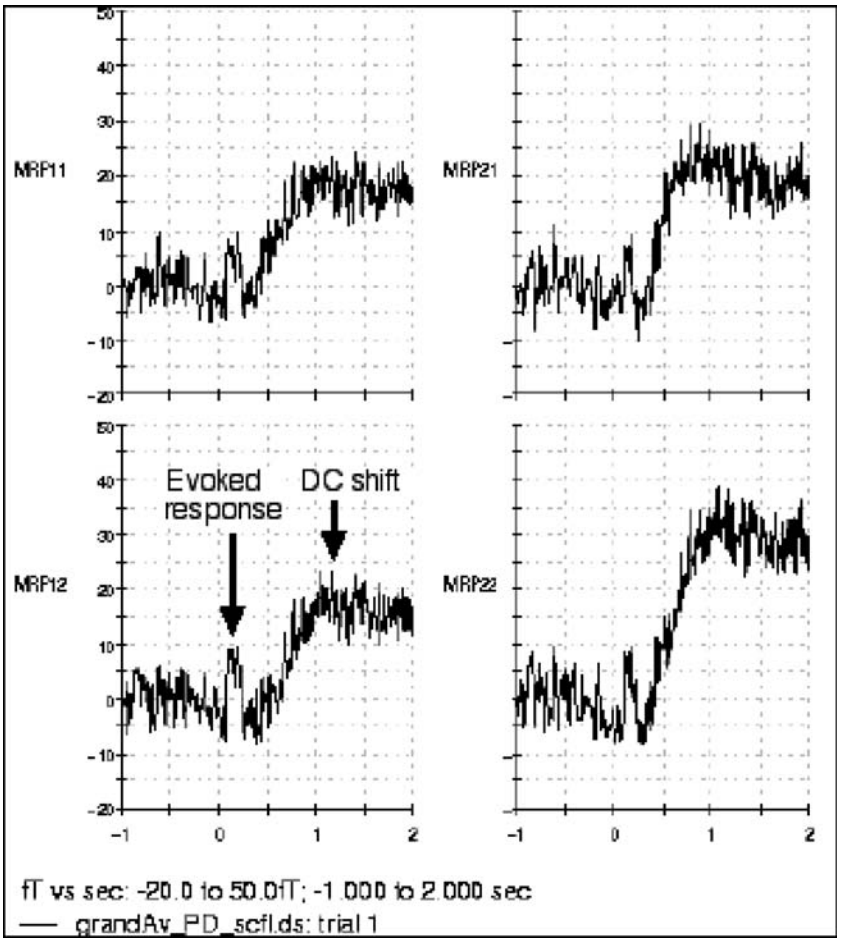

Figure 4. Data replotted from Figure 2 showing four posterior channels. Note the small evoked response (approx. 10 fT/sqrt(Hz)) located near 183 ms. Scale −20 to 60 fT/sqrt(Hz). Each trace is for the period −1.0 s to 2.0 s relative to the onset of motion coherence.

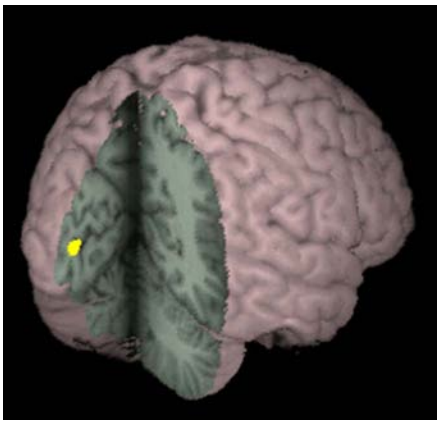

Figure 5. Preferential activation of V1 by the expansion stimulus. SnPM results for 17 participants viewing expansion vs. random motion, 3–7 Hz (theta) frequency (yellow = $p < 0.05$).

and random motion conditions in the frequency band 3–7 Hz (nominally theta). The data segments for the SAM imaging analysis were 1.0 s long, taken from the periods immediately pre- and post-stimulus onset. The figure shows the results of the non-parametric statistical analysis of the 17 individual SAM volumes using SnPM showing regions with statistically significant activation ($p < 0.05$). The results are consistent with an *increase* in power at theta frequencies for expansion with respect to random motion within the calcarine sulcus. This observation is in line with our earlier reports of an expansion bias for evoked responses to the abrupt onset of coherent motion patterns (Holliday & Meese, 2005) but now points to its anatomical locus. This is also consistent with the time course of the evoked response found in part 1, which had substantial frequency power in this spectral band.

Other optic flow stimuli are not provocative in the theta band

The other four test conditions (contraction, rotation, deformation, and translation) did not produce statistically significant activations ($p < 0.05$) in any cortical location with SnPM analysis of the results in the theta band with respect to the random motion condition.

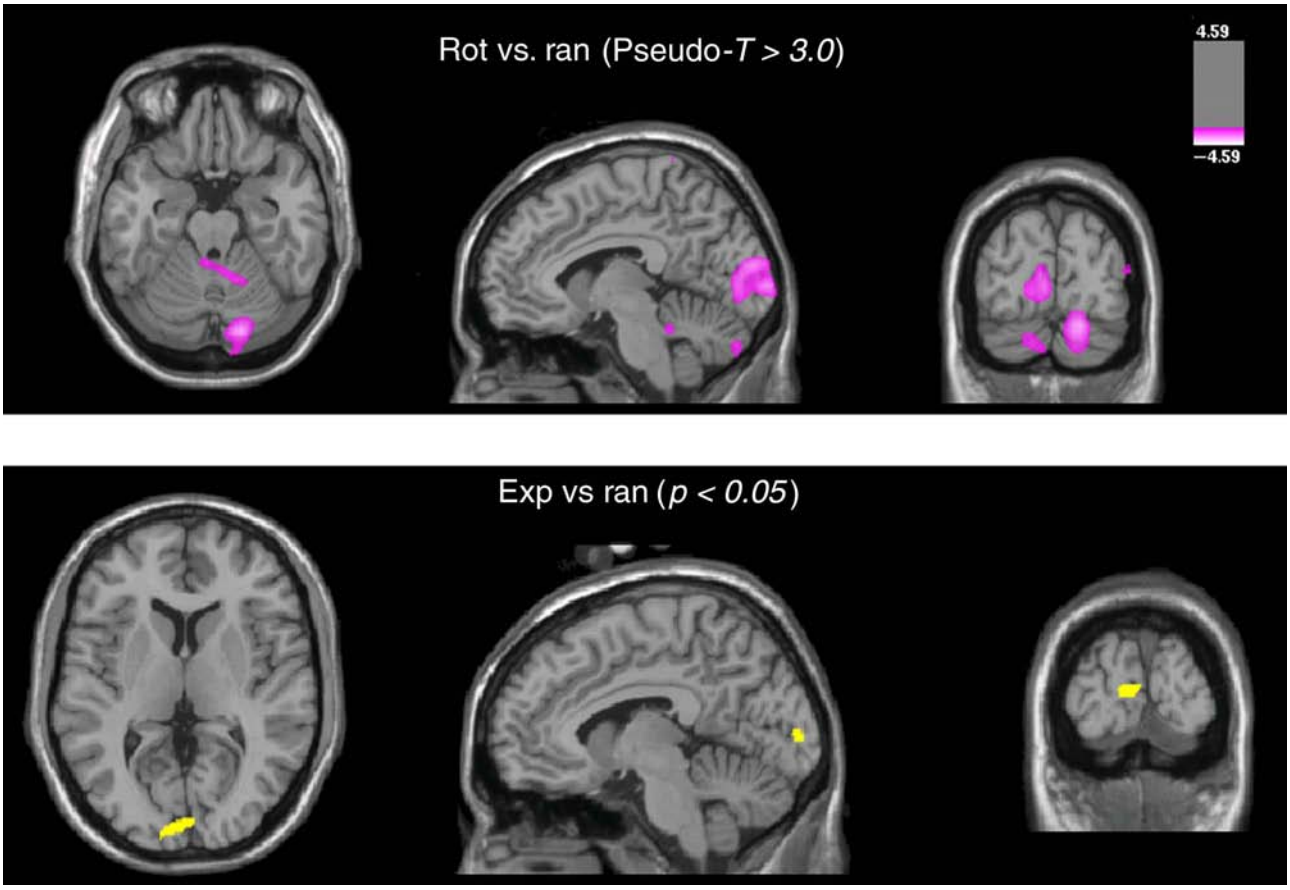

Figure 6. Different effects for rotation and expansion. Results are for SAM analysis of data from 17 participants for the theta band. Upper panel: rotation *vs.* random motion (simple effects analysis, pseudo-$T > 3.0$). Lower panel: expansion *vs.* random motion (SnPM analysis; $p < 0.05$). Frequency range of the analysis was 3–7 Hz (nominally theta band). The time windows used in the analysis were: active = 1.0 s after the onset of motion coherence; control = 1.0 s before motion onset.

In each case these observations were confirmed in an examination of a simple effects analysis of the SAM pseudo-*T* data, with the exception of rotation. For that condition, there was a *reduction* in the theta power during the period when rotational motion was presented, with SAM pseudo-$T > 3.0$ in the region around V1.

A comparison of the different results for expansion and rotation is shown in Figure 6. The data segments for the comparisons were taken for the period 0.0 s–1.0 s, from the onset of coherent motion. The upper part of the figure is for rotation *vs.* random and shows the uncorrected values from a simple effects analysis using SPM99, thresholded to show regions with the largest activation (Pseudo-$T > 3.0$). The lower panel shows the results of the more stringent SnPM analysis for expansion *vs.* random motion, as in Figure 5. Note the positive (yellow) effect for the expansion condition (bottom) and the negative (pink) effect for the rotation condition (top). However there were significant activation differences also found in the rotation vs. deformation and rotation vs. translation comparisons. In each case rotation produced a significant *reduction* in activity in comparison with the other two conditions, confirming the negative activation for rotation seen in Figure 6.

The results of all the comparisons between conditions in the theta region are presented in Table 1. Locations are shown of significant ($p < 0.05$) peaks of activation from an SnPM analysis. Activation volumes less than 7 voxels were eliminated.

Part 3. SAM analysis: Beta (17–23 Hz)

Effects were more widespread across experimental conditions in the beta band (nominally 17–23 Hz) than in the theta band. There was a reduction in oscillatory power when the response to each motion condition was compared to the random motion condition. In the terminology introduced by Pfurtscheller (2001) we might refer to this effect as an event-related de-synchronization (ERD), as to be expected when an oscillatory network is engaged in signal processing. The power reduction within the beta band was apparent in the responses of all participants, however the results of individual SAM analyses were variable, and an analysis based on grouped data proved most effective in interpreting the results.

Extensive beta-band responses for structured motion

The statistical significance of the results for the test conditions *vs.* random was assessed using SnPM (statistical non-parametric mapping). Statistical maps were produced by comparing the experimental sample with the null distribution obtained from 512 randomized permutations of the 17 result images with a confidence level set typically at $p < 0.05$. The one exception to this was for the comparison between random motion and the combined response to all of the optic flow components where, not surprisingly, the effects were most spatially extensive. In

Condition	*Grp*	*Size*	*T*	*p*	*X*	*Y*	*Z*	*X*	*Y*	*Z*	Brain region	*BA*	*R*	±
ExpvRan	A	79	5.80	0.004	−7	−89	1				Lingual Gyrus	17	20	+
	B	8	4.74	0.025				10	−75	5	Lingual Gyrus	18	2	+
ExpvCon	C	54	5.33	0.004	−4	−92	1				Lingual Gyrus	17	1	+
	D	38	5.25	0.004				16	−79	−14	Declive	*	1	+
	E	41	5.06	0.008	−9	−78	−25				Pyramis	*	1	+
ExpvRot	F	1307	6.26	0.002				21	−78	5	Cuneus	17	1	+
			6.21	0.002				16	−79	−11	Declive	*	1	+
			6.10	0.002	−9	82	12				No gray matter			
	G	<7												
RotvDef	M	177	5.47	0.006	−1	−77	0				Lingual Gyrus	18	5	–
RotvTra	N	331	6.17	0.004				24	−74	17	Precuneus	31	4	–
			5.43	0.002				18	−71	−5	Lingual Gyrus	18	1	–
	O	26	5.08	0.004				40	−84	8	Mid Occip Gyrus	19	6	–
ExpvDef	I	<7												
ExpvTra	J	<7												

Table 1. Talairach coordinates of regions of significant activation for comparisons of stimulus conditions (3–7 Hz, theta band, 1.0-s analysis time windows) identified from the SAM results by an SnPM analysis of the data for 17 participants ($p < 0.05$, number of voxels ≥7). Abbreviations: BA, Brodmann area (* = BA not defined for the cerebellum); *Exp*—Expansion; *Cont*—contraction; *Rot*—Clockwise Rotation; *Tra*—Translation upwards; *Def*—deformation. *Grp*—group reference index; several locations within one group are reported by the SPM software when more than one supra-threshold peak is found within a contiguous region; Size—activated volume in mm^3, *T*—pseudo-*T* estimated by SnPM method, peak activation Talairach coordinates *X, Y, Z* (columns 6, 7, 8 are for left hemisphere locations; 9, 10, 11 are for right hemisphere, Talairach coordinates computed by transformation icbm_spm2tal). Region identification and Brodmann area labels were assigned using the Talairach daemon client (Lancaster et al., 2000). The relative sign of power change is indicated in the last column: ± condition A in the comparison A *vs.* B had greater (lesser) theta power. Analysis of the combined results over all conditions is not shown as different conditions produced different sign of response.

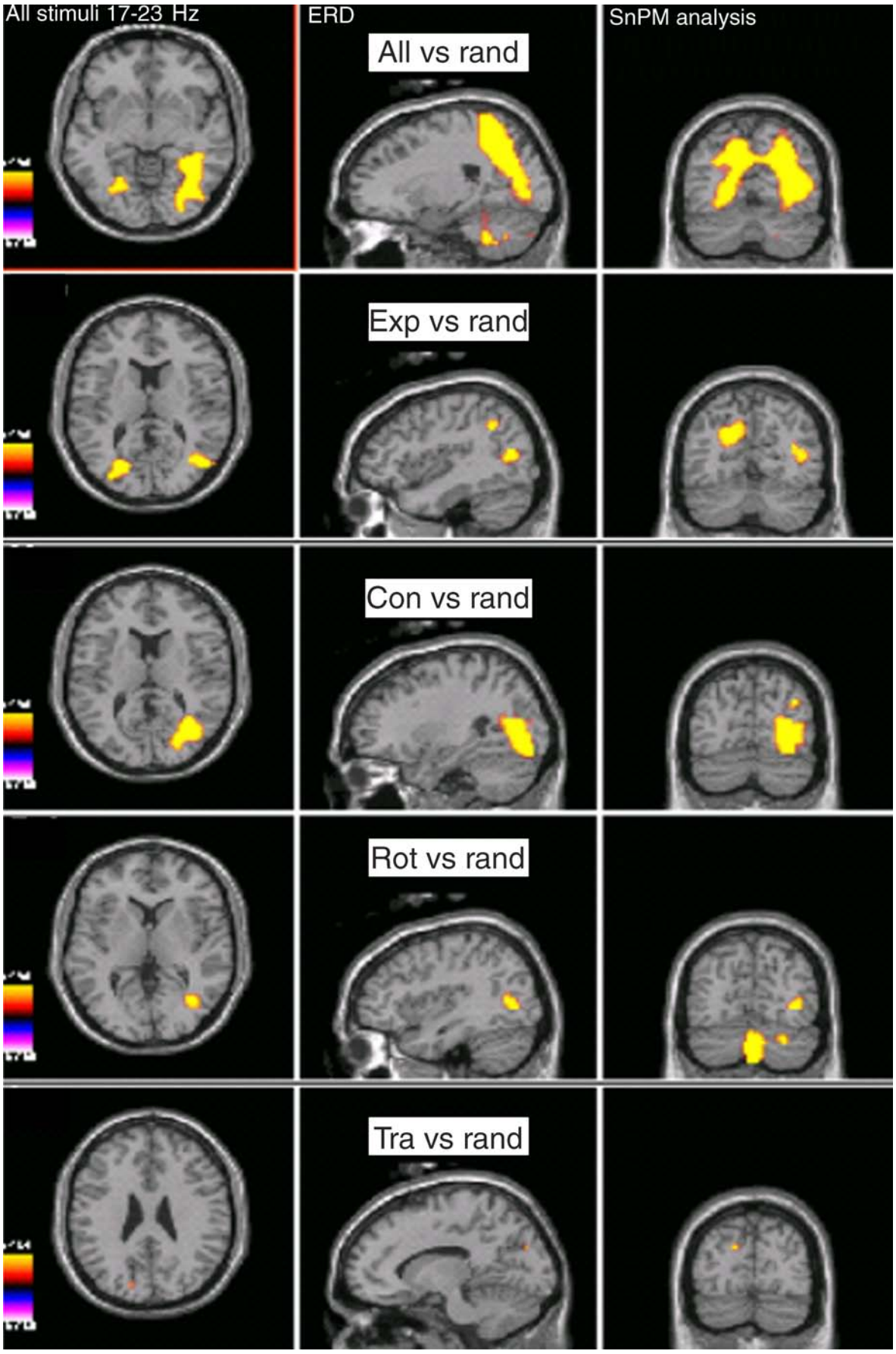

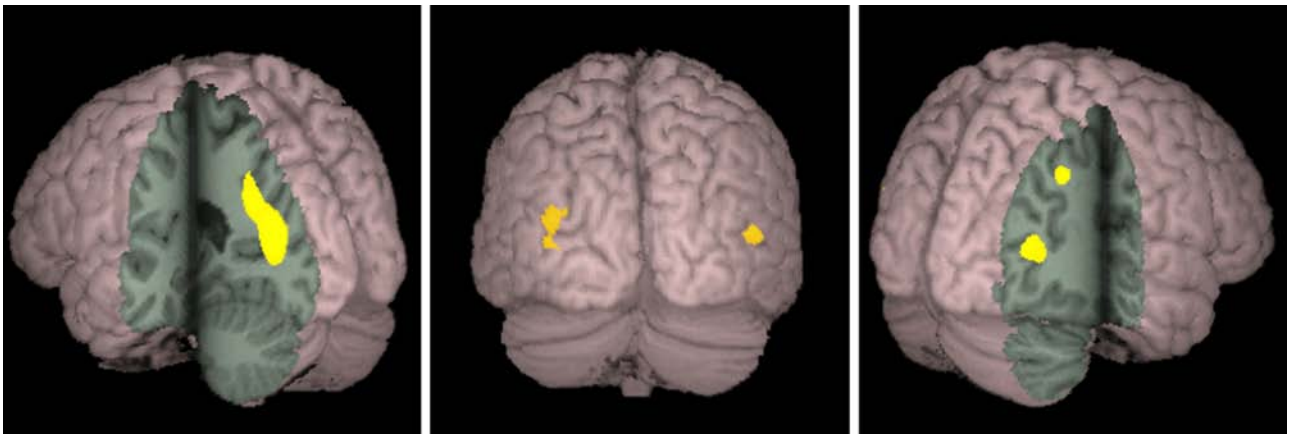

Figure 8. Expansion *vs.* random. A different visualization for the data in the second row of Figure 7. Note the bilateral activation of hMT+ in the middle panel, and activation of the posterior parietal lobes, delineated most clearly in the right panel.

this case, we were able to produce a clearer visualization of the data using a more conservative $p < 0.002$.

Figure 7 shows these SnPM results when MEG responses were averaged across all of the optic flow conditions (top row, $p < 0.002$) and for each of the individual conditions (other rows, $p < 0.05$). Regions of significant effects extended from the occipital lobe superiorly and anteriorly into the posterior parietal lobe and laterally toward the temporal lobe. More localized regions of response were produced by the individual components of expansion, contraction, rotation, and translation (Figure 7). Note that with this analysis, the expansion stimulus produced two distinct regions of response (second row, middle column), one in the posterior parietal lobe and the other in the lateral occipital region (Figure 7, row 2 and Figure 8). No significant activations were obtained for deformation, though the simple effects analysis suggested a weak presence (not shown).

Pairwise comparisons of expansion with each of the other optic flow components produced a significant result only against translation ($p < 0.05$). Even then, the region of significant activation was very small. It was located in the parietal lobe close to the midline ([3, −70, 30], BA7). Comparisons of translation against each of rotation and contraction revealed effects either outside visual areas or similar to those found against random motion. No other pairwise comparisons produced significant effects.

Figure 7. Test conditions *vs.* random. SnPM analysis of 17 participants for 17–23 Hz frequency band (beta band). The results show regions where $p < 0.002$ (top row) and $p < 0.05$ (rows 2–5) for probability of activation under the null hypothesis in an SnPM analysis. The top row shows the results when the data from all five test conditions were combined in making the comparison with random motion. The subsequent rows are for: Expansion, contraction, rotation and translation. The results for deformation were not significant. The locations of the slices were chosen to reveal the most salient activation.

As outlined in the Methods section, the anatomical locations of the activations were determined using the Talairach Daemon software (Lancaster et al., 2000). Candidate locations were obtained using the SPM99 software that identified volumes of significant ($p < 0.05$) activity then transformed from the MNI stereotaxic space to the standard Talairach space using the icbm_spm2tal transform supplied in the software package gingerALE (Laird et al., 2005). Table 2 shows the estimated locations of peak responses for the combination of all conditions, and for each of the optic flow conditions separately, *vs.* random motion. Peaks were excluded if they extended over less than 7 voxels. The group letter identifiers (A, B, C etc.) refer to contiguous regions of significant responses.

Note that a greater number of peaks and larger volumes of contiguous response were found in the right hemisphere than in the left. For the individual optic flow components the greatest contiguous volume was for the contraction stimulus (group G, Table 2) by a considerable margin (see also Figure 7, row 3). (Recall that the volume for the pooled response ('all') is based on the more conservative $p < 0.002$ and is thus markedly smaller than it would be with $p < 0.05$.) Note also that both contraction and expansion produced peaks in parietal regions (Table 2, groups F and H), which is characteristic of the pooled ('all') response (Table 2, group A; Figure 7). In contrast, rotation produced no significant parietal peaks at all. This does not mean that rotation makes no contribution to the pooled response, but that our rotation stimulus did not reveal a parietal area dedicated to this component of optic flow.

One unexpected finding was the cerebellar response to rotation. This was highly significant ($p < 0.004$) and of quite substantial volume (Table 2, group K).

Spiral space and hMT+

Several of the activations in Figure 7 are quite extensive or involved multiple regions, but in general the significance maps were not co-extensive. This is shown more

clearly in Figure 9 where the regions with significant responses for expansion, contraction, and rotation (each contrasted with random motion) are shown overlaid in red, green, and blue, respectively, and added together where they overlap. The intersection of the three SPMs is the white region indicated by the pink arrow in each panel. Note that there is just a single region of intersection. In other words, this is the only area of the human brain detected in our experiment that is selective for all three components from spiral space. The Talairach coordinates for this area [37, −62, 6] are consistent with hMT+, though in the discussion we propose the more specific label, hMSTs, with the post-fixed 's' indicating spiral-space selectivity. Importantly, this region had no significant selectivity for deformation or global translation (see Table 2 and Figure 7).

Part 4. SAM analysis: Alpha (8–13 Hz) and gamma (30–70 Hz)

SAM analyses were also conducted for the 8–13 Hz range (nominally alpha) and 30–70 Hz range (nominally

Condition	Group	Size	*T*	*p*	*X*	*Y*	*Z*	*X*	*Y*	*Z*	Brain region	BA
All	A	1644	7.79	0.002				35	−64	7	No gray matter found	19
All			7.21	0.002				23	−62	42	Superior Parietal Lobule	7
All			6.71	0.002				18	−52	59	Superior Parietal Lobule	7
All	B	516	6.22	0.002	−18	−59	39				Precuneus	7
All			5.69	0.002	−7	−72	30				Precuneus	7
All			5.68	0.002	−10	−77	21				Cuneus	18
All	C	28	5.71	0.002				24	−43	−35	Cerebellar Tonsil	*
Exp	D	353	5.45	0.002	−24	−76	13				Cuneus	17
Exp			5.12	0.004	−18	−66	22				Precuneus	31
Exp			5.01	0.006	−10	−69	25				Precuneus	31
Exp	E	55	5.04	0.006				43	−70	9	Middle Occipital Gyrus	19
Exp			4.64	0.039				32	−65	15	No gray matter found	
Exp	F	17	4.99	0.006				37	−53	35	Inferior Parietal Lobule	40
Cont	G	1840	7.12	0.002				24	−74	−5	Lingual Gyrus	18
Cont			5.94	0.002				16	−87	−17	Post. Lobe/Fusiform Gyrus	*
Cont			5.82	0.002				18	−79	11	Cuneus	17
Cont	H	90	5.28	0.008				20	−66	52	Superior Parietal Lobule	7
Cont	I	18	4.64	0.019				4	−74	19	Cuneus	18
Cont	J	43	4.63	0.019	−21	−60	20				Posterior Cingulate	31
Cont			4.45	0.045	−10	−60	28				Precuneus	31
Rot	K	701	5.71	0.004				2	−63	−37	Inferior Semi-Lunar Lobule	*
Rot			5.39	0.004				13	−55	−30	Nodule	*
Rot	L	282	5.56	0.004				35	−67	4	No gray matter found	
Rot			5.13	0.004				24	−80	−6	Lingual Gyrus	18
Rot			4.92	0.006				29	−91	−12	Fusiform Gyrus	18
Tra		<7										
Def				n.s.								

Table 2. Talairach coordinates of regions of activation for each optic flow condition *vs*. random motion (17–23 Hz (beta-band), 1.0-s time windows) identified from the SAM results by an SnPM analysis of the data for 17 participants ($p < 0.05$, number of voxels ≥7). In all cases the values showed reductions in power within the beta frequency range. Abbreviations: BA, Brodmann area (* = BA not defined for the cerebellum); *All*—All conditions; *Exp*—Expansion; *Cont*—contraction; *Rot*—Clockwise Rotation; *Tra*—Translation upward; *Def*—deformation. Group—reference index; several locations within one group are reported by the SPM software when more than one supra-threshold peak is found within a contiguous supra-threshold activated volume; Size—activated volume in mm^3, *T*—pseudo-*T* estimated by SnPM method, peak activation Talairach coordinates *X, Y, Z* (columns 6, 7, 8 are for left hemisphere locations; 9, 10, 11 are for right hemisphere, Talairach coordinates computed by transformation from MNI coordinates with icbm_spm2tal). Region identification and Brodmann labels were assigned using the Talairach daemon client (Lancaster et al., 2000). Contiguous regions were defined using SnPM analysis for a statistical threshold of $p < 0.05$ in all conditions except for the *All* condition, where $p < 0.002$. The *p*-values reported in the table are for the peak activities.

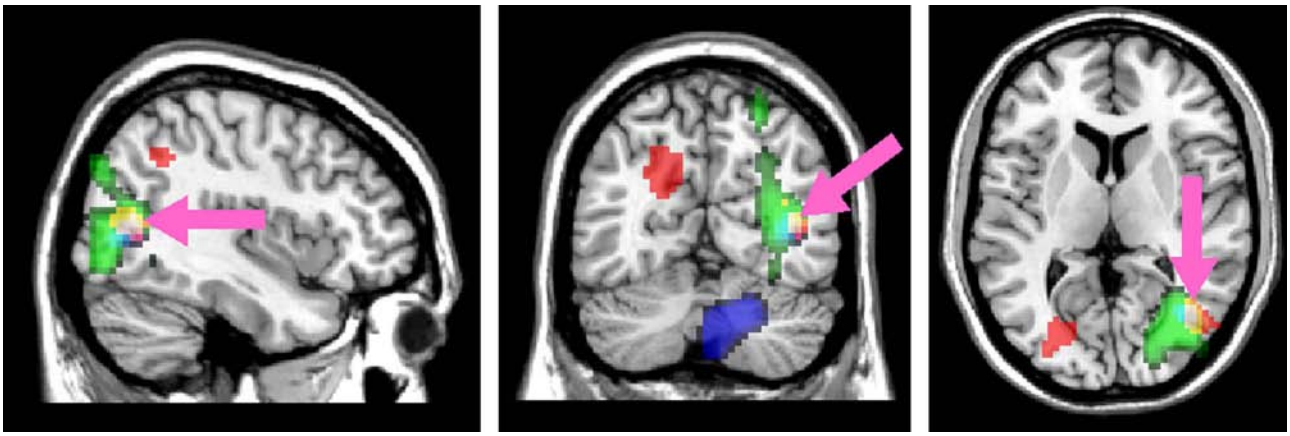

Figure 9. A brain region for spiral space. SnPM analysis ($p < 0.05$) for 17 participants (beta band) for expansion vs. random (red), contraction vs. random (green), and rotation vs. random (blue). The Talairach coordinates for the region of intersection (white, highlighted by the pink arrow) are: [37, −62, 6], consistent with the location of hMT+. We refer to this region as hMSTs.

gamma). In both cases the results obtained were generally consistent with the observations within the beta band (a reduction in power), but with smaller amplitude at some locations, or producing no effects at all. These effects are most likely accounted for by supposing that the alpha and gamma frequency bands permitted a limited observation window into the main beta-band functional response that was more diffuse than the narrow 17–23 Hz window used in our analysis. That is, the alpha and gamma analysis windows partially overlapped the low- and high-frequency portions of the beta response band, respectively.

Discussion

The results reported here support and extend earlier observations of optic flow analysis in the human cortical visual system. Our principle findings fall under three headings as follows:

1. Low-amplitude evoked responses to the onset of motion coherence and a slowly accumulating maintained DC magnetic field.
2. An expansion bias in the calcarine sulcus (V1) in the low-frequency theta band (3–7 Hz).
3. Widespread extra-striate responses within the mid-frequency beta band (17–23 Hz), encompassing the region around hMT+ and extending into the occipito-parietal cortex along the intraparietal sulcus (IPS).

The only region of the brain to respond to all of the components from spiral space was hMT+. Rotation produced a selective response in the cerebellum. We found little or no selectivity for deformation or global translation anywhere in the brain. We discuss each of these findings below.

Part 1. MEG evoked responses

When averaging was applied to the measured MEG signals for individual conditions or participants there was no evoked response, as anticipated in our design using continuous motion displays. However when we combined data across participants and conditions, thus greatly reducing the residual noise power (3,400 trials), to our surprise two new observations were obtained.

Firstly, very small evoked responses were present, indicating phase-locked brain responses to the onset of the coherent motion stimuli. The time course of this response showed an initial emergence from the noise level at about 150 ms after the onset of motion coherence, peaking at about 183 ms. At this time the magnetic field was symmetrically distributed over the sensor array, with the strongest fields over the posterior sensors, consistent with one or more sources near the midline in the parietal region (see Figure 2, top right). These results are concordant with other reports on motion onset evoked responses (Ahlfors et al., 1999; Prieto et al., 2007), and with our own observations with similar stimuli to the experiment reported here (Holliday & Meese, 2005). We speculate that the brief evoked response at 150–180 ms is due to the onset of structured motion in the first frame of the stimulus, or thereabouts. Because the lifetime of the dots was 10 movie frames (equal to two video refresh frames) and there were 200 dots in all, this is equivalent to 20 dots (10%) moving coherently at the first time step of the structured motion sequence, which is at or just above psychophysical coherence threshold for these stimuli (Meese & Harris, 2001b; Morrone et al., 1995). Recently, several groups have studied motion coherence using neuroimaging methods, and in particular the results of Donner et al. (2007) bear a striking relation to those here. They measured magnetic evoked responses to motion with the signal level set to each participant's psychophysical

coherence threshold (these ranged from 4.5 to 10.5% for the 4 participants in their study). Like us, they also observed an evoked response component for their stimuli. Interestingly, they also required a substantial number of trials (up to 6,000) in order to reveal these very small effects with their low coherence stimuli. Donner et al.'s main analysis examined induced responses and demonstrated that they were predictive of task performance (detection). However, it is interesting to note that prediction reliability increased slowly over several seconds during the observation period, with a time course similar to the DC trend we found here, as we now describe.

The second observation here was of "DC-shifts" that accumulated over a period from 0.5 s after stimulus onset to the end of the recording period for each stimulus. Sustained fields or "DC-shifts" have been reported before with visual stimuli. For example Brookes et al. (2005) demonstrated sustained MEG activations during presentation of high contrast grating stimuli frequency by extracting the analytic signal or envelope (Bracewell, 1986) of the DC, alpha and gamma bands. Similar sustained MEG responses have also been reported during migrainous visual aura (Hall et al., 2004). One interpretation of these results is that the sustained field reflects a sustained cortical current produced by the ongoing visual stimulation. However the change in the magnitude of the sustained field obtained with the onset of coherent motion from the random motion baseline was extremely small (about 40 fT/sqrt(Hz)).

In the following sections we discuss the results of the SAM analysis, which revealed much larger effects in different frequency ranges and in several regions of the visual cortex.

Parts 2 and 3. SAM analysis

Three separate regions of the cerebral cortex were identified in response to optic flow components by comparison to stimulation by random motion: the region within or near the calcarine sulcus, indicating the involvement of primary visual cortex (V1); inferior lateral occipito-temporal cortex, consistent with activation of the human homologue of the macaque MT complex (V5 or hMT+); and within the occipito-parietal region in the vicinity of the superior parietal lobule and the intraparietal sulcus (IPS).

The regions activated differed in the frequency ranges in which stimulation was effective, as described below.

Foveo-fugal response bias in the theta (3–7 Hz) range for V1

Within the 3–7 Hz frequency band used for SAM source analysis (here nominally 'theta') only the expansion condition was effective in generating a response, producing increased power with respect to the random motion condition. The region of cortex most strongly activated within this frequency range was in and around the calcarine sulcus (Figures 5 and 6), indicating an involvement of the primary visual cortex (V1). This was the only brain region that showed a selective response in this frequency band for the comparison with the random motion condition. SAM source analysis suggested that rotational motion (orthogonal to expansion) produced a *reduction* in theta power (pseudo-$T > 3.0$), but this effect did not reach statistical significance ($p = 0.15$) when applying SnPM non-parametric analysis.

Many neurons in primary visual cortex (V1) are directionally selective for motion and have small receptive fields supporting motion processing at a local level. Large receptive fields for global image analysis are unknown in this area, so how might a bias emerge for the global expansion pattern used here? One possibility is that the preferred directions of the local mechanisms are not evenly distributed across the visual field (and V1) but are biased (in number or sensitivity) toward the foveofugal directions (i.e., radiating out from the center of the fovea). In fact, there is good psychophysical evidence for such a bias. Georgeson and Harris (1978) used patches of counter-phase sine-wave gratings, which are equivalent to two superimposed grating patches moving in opposite directions at equal speed. However, when viewed in the periphery, observers reported that one of these drift directions dominated perception: the one drifting away from the fovea. Thus, our results here suggest that the anatomical locus of the effect found by Georgeson and Harris (1978) is as early as primary visual cortex.

A foveo-fugal bias has also been found among direction selective visual neurons in monkey cortex (Albright, 1989). However, this was in MT, and more likely relates to the more appropriately placed expansion biases that we found in the beta band (group E, Table 1), if at all.

The theta results here are also consistent with those of Holliday and Meese (2005). They found that the evoked response to the onset of motion from static dots was slightly greater for expansion than for other optic flow components. It seems likely that the substantial evoked responses in that study were driven largely by the onset of motion, regardless of stimulus type (see previous subsection). Nevertheless, it would also seem that the theta-band expansion bias here, which we presume to be related to the evoked response (see Results), remained visible in the results of the previous study, superimposed on the more general evoked response to stimulus onset. In agreement with others (Georgeson & Harris, 1978; Holliday & Meese, 2005), we suggest that this expansion bias reflects our exposure to the radiating patterns of optic flow that are experienced as we navigate the world, primarily moving forward (Brosseau-Lachaine, Casanova, & Faubert, 2008; Ivins, Porrill, Frisby, & Orban, 1999; Zanker & Zeil, 2005).

It is also of interest to compare this motion bias with what seems like a related bias found in spatial vision. Rovamo, Virsu, Laurinen, and Hyvärinen (1982) found that spatial acuity was greater for patches of sine-wave grating arranged such that their contours radiated out from the center of the fovea. Similarly, Meese and Williams (2000) found that contrast sensitivity to patches of 5 c/deg grating was greater for the radiating configuration than for a configuration at right angles to this. However, although both the motion and spatial biases emphasize radiation (of motion direction or contour orientation) away from the center of the fovea, the local receptive fields that are needed would have to be oriented at right angles to each other: parallel to spatial contours, and orthogonal to the direction of motion. This implies that the motion and spatial biases are carried by independent sets of neural mechanisms.

Extra-striate activations in the beta (17–23 Hz) range: hMT+ and the IPS

In the beta frequency region there were two main activated cortical volumes, one in the extra-striate cortex, lateral to the primary visual cortex, and the other in the region of the anterior part of the IPS. When the MEG responses were averaged across all five global motion conditions and compared against random motion, a substantial volume of occipito-parietal activation was found (Figure 7; group A in Table 2), indicating the importance of structured motion in this pathway. It is noteworthy that the expansion and contraction stimuli (Figure 7) appeared to contribute most substantially to this volume (see also Table 2), though no significant differences between complex motions were found. In fMRI studies Könönen et al. (2003) found substantial activation in this parietal region using a small-field (7.5° × 7.5°) rotation stimulus and Wall and Smith (2008) have implicated this area with ego-motion.

Significant effects were found for several of the individual global components compared with random motion (Figure 7). However, if the only critical factor were the local/global distinction, then the translation and deformation components should have been as potent as the spiral-space components. This was not the case; they produced only weak or no significant effects. Thus, our results cannot be understood in terms of either medium-sized mechanisms that prefer (unidirectional) motion across a region of several dots, or more general mechanisms involved in the response to any form of coherent motion. Instead, our data reveal a distinct overall preference for the optic flow components that form spiral space. However, only a single region in the entire brain responded to all three of the spiral-space components (Figure 9). This selectivity cannot be understood in terms of topographical biases such as those that we found in V1. For example, the combination of a foveo-fugal bias, a foveo-petal bias, and corresponding biases for local directions orthogonal to these results in no overall bias at all. Thus, our optic flow stimuli must have excited mechanisms that are dedicated to their representation. Here we use this unique and exclusive selectivity for spiral space to define this area as hMSTs (where the appended 's' stands for spiral space).

Other considerations indicate that this region may be the human homologue of MST rather than MT. For example MT receptive fields are much smaller than those in MST and, presumably, would respond to the individual dots in our low-density random motion stimuli (see Methods section). Thus if hMT were sensitive to our control stimulus then it is unlikely that our test stimuli would result in strong comparative responses, making hMT an unlikely candidate. On the other hand, several other studies have claimed to identify hMT based on comparisons across global translation and random motions. Most of those studies (see Table 3) used much higher dot densities than that used here, though Morrone et al. (2000) used a very similar density to us. But even if typical receptive fields in hMT were sufficiently large to be unresponsive to the (more local) random motions because of spatial pooling, the deformation and translation components should have been as potent as those from spiral space, as we argued above, and they were not. In contrast, the dorsal part of MST (MSTd) in monkey has long been associated with global complex motions in single-cell physiology (Duffy & Wurtz, 1991a; Graziano et al., 1994; Lagae, Maes, Raiguel, Xiao, & Orban, 1994; Orban, Lagae, Raiguel, Xiao, & Maes, 1995; Tanaka & Saito, 1989), albeit with a bias toward expansion (Anderson & Siegel, 1999; Geesaman & Andersen, 1996; Graziano et al., 1994; Heuer & Britten, 2004; Tanaka, Fukada, & Saito, 1989; Tanaka & Saito, 1989). More recently, fMRI studies on humans have also made this association (Morrone et al., 2000; Smith et al., 2006; Wall & Smith, 2008).

From an anatomical point of view, however, there are some small but curious disagreements among studies. Those studies for which we were able to establish Talairach coordinates for the putative location of human MT+ in the right hemisphere for comparison with our results are summarized in Table 3. When necessary, published coordinates were transformed into the standard Talairach system using gingerALE, a software package designed for this purpose as indicated in the table caption (Laird et al., 2005). There is considerable agreement on the lateral x-coordinate (range 10.2 mm), but greater variation in the y- (anterior/posterior) and z- (dorsal/ventral) coordinates (ranges 23.2 mm and 16.4 mm, respectively). In an anatomical study, Annese et al. (2005) showed the 3-D reconstruction of left and right hemispheres for hMT based on the myelo-architecture from a single human brain (we consider hMT+ a more appropriate label for this structure). The coordinate extremities for the right hemisphere are shown toward the bottom of Table 3. These are quite extensive, but they envelop the mean location of the functional imaging

Study	Area	Method	Motion stimuli (Target/control)	*N*	*X*	*Y*	*Z*	*r*	Trans.
This study	hMSTs	MEG	SS/Rnd	17	36.7	−62.3	6.2	6.2	icbm
Siegel et al. (2007)	hMT+	MEG	Tran/Rnd	7	46.0	−67.0	0.0	6.1	no
Martinez-Trujillo et al. (2007)	hMT	MEG	Tran dir-ch	9	37.4	−63.8	14.7	12.6	unB-icbm
Wall et al. (2008)	hMT	fMRI	Exp&Rot/Stc	6	44.0	−66.0	0.0	4.3	no
Wall et al. (2008)	hMST	fMRI	Exp&Rot/Stc	6	45.0	−62.0	0.0	4.8	no
Giaschi et al. (2007)	hMT+	fMRI	Exp&Cont/Stc	6	39.0	−60.0	−1.0	5.9	no
Braddick et al. (2001)	hMT	fMRI	Tran/Rnd	3	45.0	−70.3	1.1	7.5	icbm
Morrone at al. (2000)	hMT	fMRI	Tran/Rnd	4	35.8	−62.0	3.5	6.1	icbm
Morrone et al. (2000)	hMST	fMRI	SS dir-ch/Rnd	6	41.4	−60.6	−1.7	5.5	icbm
Dumoulin et al. (2000)	hMT	fMRI	Check/Stc	9	39.5	−64.4	−1.2	4.4	icbm
Paradis et al. (2000)	hMT+	fMRI	Rnd/Stc	9	40.4	−52.8	5.4	11.4	icbm
Ahlfors et al. (1999)	hMT+	fMRI	Exp&Cont/Stc	3	41.0	−59.0	6.0	5.8	no
Tootell et al. (1995)	hMT	fMRI	Exp&Cont/Stc	18	45.0	−76.0	3.0	12.7	no
Ptito et al. (2001)	hMT	PET	Rnd/Stc	5	46.0	−64.0	3.0	4.5	no
Watson et al. (1993)	hMT	PET	Tran dir-ch/Stc	12	41.0	−67.0	2.0	3.3	no
Malikovic et al. (2007)	hMT+	Stain	–	4: ≤10	49	−70	11		
Annese et al. (2005)	hMT	Stain	–	1	25: 47	−89: −64	−18: 5		
Average (mm)	hMT+	Imaging	–	111*	41.6	−63.8	2.7		
Range (mm)	hMT+	Imaging	–	–	35.8	−76.0	−1.7		
					46.0	−52.8	14.7		
SD (mm)	hMT+	Imaging	–	–	3.5	5.3	4.2		

Table 3. Talairach coordinates for hMT, hMT+, and hMST(s) within the right cerebral hemispheres from several studies. (Authors have not used the labels hMT and hMT+ consistently, and the reader is referred to the original papers for details. Where the label V5 was used in the original work, this has been replaced with hMT here for consistency.) The two studies at the bottom of the table used anatomical staining of brains from deceased humans. The remaining studies involved functional imaging of brains of normal human volunteer participants. The statistics in the bottom three rows were derived from the figures in the first fifteen rows. The data from Wall et al. (2008) were provided for us by personal communication. We have omitted an entry for a MEG study by Händel, Lutzenberger, Thier, and Haarmeier (2007) because of the complexity of the data set. *N* = the number of brains reported in the studies. *We have assumed no participant took part in more than one study. *X, Y, Z* = Talairach stereotaxic coordinates (mm). *r*—Euclidian distance from each published MT location to the mean location (mm). Trans. = Transformation applied to published results with gingerALE, a software package available from the Research Imaging Center of the University of Texas Health Science Center San Antonio [http://brainmap.org/index.html]: icbm—icbm_spm2tal; unB-icbm—inverse Brett transform, then icbm_spm2tal; no—no transformation applied (Laird et al., 2005). Stimulus abbreviations. SS: spiral space; Exp: expansion/outward radiation; Cont: contraction/inward radiation; Rot: rotation; Tran: translation; Rnd: random; Stc: static (no motion); Check: jittering checkerboard; dir-ch: change in direction.

studies. It is perhaps worth noting that in this anatomical study the region identified as hMT extended considerably in the posterior direction (to $x = -89$ mm) compared to the result of the functional imaging studies ($x = -76$ to -52.8 mm) and was typically centered on a gyral crown not in the sulcal wall or floor as is often reported in functional imaging studies. Thus, it seems plausible that these other studies tapped different subdivisions of hMT+. Indeed, using fMRI, Morrone et al. (2000) found a functional distinction between hMST, which responded to spiral space, and hMT, which responded to translation. On average, they found hMST to be about 6 mm ventral to hMT. However, other imaging studies that have distinguished hMT and hMST with regard to their contra-/ipsi-lateral drive and retinotopy (Huk et al., 2002; Smith et al., 2006; Wall & Smith, 2008) have found the distinction to be more marked along the anterior/posterior (y) dimension (hMST being more anterior), with little or no ventral difference (an example shown in Table 3 is Wall et al. (2008)). Cytoarchitechtonic differences within this region have been described as dorsal and ventral (Malikovic et al., 2007, Figure 2) though, from the images shown, there is also a considerable lateral displacement of these regions into the sulcus. Our hMSTs tends toward the anterior end of the spread in Table 3 (i.e., less negative y), consistent with the Huk and the Smith studies, but also the more dorsal end of the spread (more positive z), quite unlike the Morrone study. Indeed, our own hMSTs is closer to the region identified as MT than MST by Morrone et al. by some 6 mm.

Some caution must be made in interpreting point location estimates of what are rather extensive cortical regions; an estimate of 719 mm^3 is given by Malikovic et al. (2007) for the 4/10 overlapped volume of the region hOc5 (possibly associated with MT+) in the brains they examined. It could be that the heterogeneity of the results arises from anatomical differences among the participants

in the different studies, which can vary in the order of 1 or 2 cm when functionally defined (Martinez-Trujillo et al., 2007; Morrone et al., 2000; Smith et al., 2006; Watson et al., 1993) and, seemingly, also when defined by anatomical staining (Annese et al., 2005; Malikovic et al., 2007). Another possibility is that hMT+ involves more than two areas with different specialisms, which is responsible for some of the differences in Table 2 owing to the different methodologies that have been used. Indeed, four motion sensitive sub-regions have been identified in the dorsal superior temporal sulcus of macaque: MT, MSTd, MSTl, and FST. But whatever the case, the region that we refer to here as hMSTs is within 6 mm of the average hMT+ from the imaging studies in Table 3, which is slightly less distant than the standard deviation across those studies (average *SD* 7.6 mm from Table 3).

Lateralized responses to optic flow

From Figure 7 and Table 2 it is clear that the left hemisphere was generally less responsive than the right. Similar asymmetries in responses to motion have been reported before. For example, in a MEG study, Martinez-Trujillo et al. (2005) found a right-lateralized response in the inferior parietal lobe while participants were performing a direction discrimination task. Kleinschmidt et al. (2002) found a right-hemisphere dominance using a rotating windmill stimulus. Prieto et al. (2007) found that all hMT+ activations were lateralized: in four participants this was in the right hemisphere but in the other four it was in the left hemisphere. In our study, several participants showed striking response symmetry (not shown), causing us to question whether the evidence here argues for hemispheric specialization for motion processing. One possibility is that there is greater variability in the cortical locations of motion mechanisms in the human left hemisphere than the right (see for example Amunts et al., 2007). That would lead to a weaker response in the left hemisphere when results are averaged across participants.

Rotation and the cerebellum

A result that we had not anticipated was the selective involvement of the cerebellum in response to the rotation stimulus. A detailed understanding of this requires further investigation, but a few comments are in order here. Our large (70 deg diameter) stimuli produced a sense of vection during the onset of coherent motion. For expansion and contraction this was passive motion toward and away from the display, whereas for rotation one sensed the body rolling in a direction opposite to that being displayed. Thus, we envisage that mechanisms involved in compensating for body roll (or fall) would be primed by our rotation stimulus. Exactly what processes might be involved is not clear, but we note that rotating displays also influence gait (Richards et al., 2004), which is associated with the cerebellum (see Jahn et al. (2008) for a recent example), and that this structure has been associated with postural responses to full field motion (Slobounov et al., 2006). Thus, the visual rotation here might activate a visuo-cerebellar pathway that has a similar role to that of the vestibular-cerebellar pathway (e.g., see Cinelli, Patla, & Stuart, 2007). We also note that Kleinschmidt et al. (2002) found that a large field rotation stimulus could induce vection and that the only brain region that responded selectively to this sensation (using fMRI) was the cerebellar nodulus. Finally, we note that work on patients with cerebellar lesions has found performance deficits for discriminating direction for coherent motion (Jokisch, Troje, Koch, Schwarz, & Daum, 2005), though how this relates to the rotation specific finding here is not clear.

Deformation and the issue of speed gradients

We found no evidence for an area of the brain that responded selectively to deformation against either random motion or any of our other optic flow components. Our results and analysis point to a clear preference for the components from spiral space, but this does not preclude the possibility of a specialization for deformation. It could be that such mechanisms are to be found in the area that we have identified as hMSTs, but that they are far fewer in number and did not achieve the requisite signal-to-noise ratio to be revealed by our analysis. Indeed, physiological investigations have found fewer cells with a preference for this type of stimulus than those preferring other optic flow components (Lagae et al., 1994). It is also possible that visual architecture is not arranged to 'pick up' pure deformation stimuli, but instead is sensitive to conjoint activations of deformation with components from spiral space and translation, consistent with those encountered in structured environments (Ivins et al., 1999; Meese et al., 1995). Further work is needed to address this possibility.

Another possibility is that the presence of speed gradients (a change in speed against space) might be critical for the deformation stimulus. Speed gradients in deformation-related stimuli appear to be important for some cells in MT (Treue & Andersen, 1996) and they also play an important role in perception of slant magnitude (Braunstein, 1968; Domini & Caudek, 1999; Meese et al., 1995): when the speed gradient is removed, perception of slant is much less compelling (Harris, Freeman, & Hughes, 1992). This is also consistent with our informal observations of the stimuli used here, where no speed gradients were included. Indeed, the variation of local speed across area is central to the analysis of surface structure (Koenderink & van Doorn, 1986, 1992) and depth (Calow & Lappe, 2007). Thus, a deformation stimulus with the speed gradient reinstated might be better suited to revealing the brain regions involved in analyzing this form of optic flow.

It seems likely that the issue of speed gradients is less important for the stimuli from spiral space than those from

deformation space. Although general spiral motions do look different when the speed gradients are removed, psychophysical (Meese & Anderson, 2002), fMRI (Morrone et al., 2000), and MEG (Holliday & Meese, 2005) studies have found that the inclusion, or not, of speed gradients is a factor of little importance for basic response measures. Presumably, this is because the variation of local speed across area is of secondary importance for signaling observer roll and direction of heading (Warren, Blackwell, Kurtz, Hatsopoulos, & Kalish, 1991). Indeed, Calow and Lappe (2007) found that speed and direction were only slightly correlated in natural movie statistics and that speed distributions are related to depth structure (see above) whereas direction distributions are related to navigational requirements. It is also of some note that single-cell recordings in monkey MSTd have found that the presence of speed gradients in spiral space is of little or no importance (Orban et al., 1995), though the contrary result has also been reported (Duffy & Wurtz, 1997b).

No cortical response to global translation

In the study here, the translation component was not a provocative stimulus. We have already explained that visual analysis of local translations (such as those measured in V1 and MT) should not be expected to show up in our study because the fairly low density of our displays means these would be cancelled in the comparison with random motion. However, the general lack of evidence for a (substantial) global analysis of translation might seem surprising. For example, full-field translations arise when observers make eye movements, and one might suppose that this forms part of the general analysis of retinal flow (Lappe et al., 1999). However, it is well known that the motion that arises from eye rotations contains no useful information (e.g., Longuet-Higgins & Prazdny, 1980) and that it would be beneficial to dispose of this early on, suggesting a possible reason why it does not show up here.

Of course, large field translation arises from other sources, including head and body movements, and the movement of large objects in close proximity to the observer (e.g., woolly mammoths and buses). Retinal flow from head and body movements is always accompanied by a component of deformation (in typical environments) and is important for judgements of the magnitude of surface slant and tilt (Freeman & Fowler, 2000; Freeman et al., 1996; Meese et al., 1995). For this reason, one might expect that this source of translation is parceled with the analysis of speed gradients and combined within specialized mechanisms that were not tapped by our stimulus set here (Ivins et al., 1999). Large object motion is encountered rarely on a daily basis (regardless of historical era) and might involve scarce neuronal resources that are untouched by the sensitivity of our analysis methods.

More generally, and by analogy to the processing of luminance contrast, it is perhaps motion contrast (relative motion) that provides a richer source of information than absolute motion, and thereby more likely to be encoded (Allman, Miezin, & McGuinness, 1985; Loomis & Nakayama, 1973; Nakayama & Loomis, 1974; Snowden, 1992; Watson & Eckert, 1994; Xiao, Raiguel, Marcar, Koenderink, & Orban, 1995). Nonetheless, it is curious that cells in MSTd are known to respond well to large field translation (Duffy & Wurtz, 1997a), yet we found no evidence of that here.

Part 4. Some more comparisons with MEG studies

As mentioned earlier, Donner et al. (2007) reported MEG recordings of responses to random-dot motion where motion coherence was set at coherence threshold. They found that the beta frequency response localized in the posterior parietal region and was related to the accuracy of participants' behavioral responses. The right posterior region of the intraparietal sulcus was observed to be activated in all four participants while only two showed responsiveness in the left hemisphere. Other extra-striate activations were noted, such as MT+, but these authors state that the parietal region predominated in the cortical response to visual motion in the posterior regions of the brain. In Donner et al. (2007) and an earlier study by the same group (Siegel, Donner, Oostenveld, Fries, & Engel, 2007), increased MEG signals were reported in the high gamma frequency range (60–100 Hz), widely distributed over posterior brain regions. Though the maximum amplitude of gamma activity was localized in the early visual areas (V1/V2/V3) there was no relationship of the gamma response to motion coherence, though this was the case for hMT+ and the occipito-parietal cortex. In our study we observed no specific effects in the gamma frequency range. This may be due to the different stimulus and task design. In the case of Siegel et al. (2007) the stimulus was presented abruptly from a blank screen, whereas in our design the motion patterns emerged gradually from unstructured random motion. However, more simply, it may be due to the greater statistical power used in the experiments of the Hamburg/Nijmegen group who used data combined from up to 6000 trials for each of their participants to detect the very small gamma-band effect. Nevertheless both their studies and ours indicate that the posterior parietal cortex is a key node in the cortical visual network (see also Martinez-Trujillo et al., 2007) and that MEG responses in the beta frequency range are characteristic of activity in the dorsal pathway.

Conclusions

The power and scope of this study compared with several previous imaging studies (mainly fMRI) owes to (i) our use of a more complete set of optic flow stimuli,

(ii) the absence of stimulus onset transients that might otherwise have caused masking, and (iii) the use of fine time-scale analysis using MEG and SAM.

MEG responses in the theta band (3–7 Hz) were predominantly within the posterior occipital regions (V1) but represented substantial increases in signal power only for the expansion stimulus. Expansion-related biases are abundant in the vision literature, but until now their origin in human vision has remained elusive. Here we have shown that it precedes the elaboration of more complex neural machinery tailored to its coding, and ascribe it to a foveo-fugal (outward-radiating) bias of unidirectional motion sensors in V1.

As reported in some other studies we found a greater response to coherent motion in the right hemisphere. We also found that extra-striate occipital and occipito-parietal regions showed the strongest effects, characteristically reducing oscillatory power in the beta band (17–23 Hz).

Perhaps most importantly we have provided the first demonstration of exclusive spiral-space selectivity in hMT+, which we use to define the sub-region hMSTs. This result suggests a functional role for this region better suited to the preliminary analysis of ego-motion than surface pose, which would have necessarily involved the deformation component that we found ineffective in eliciting a response.

The substantial activity that we found in the dorsal stream around the IPS emphasizes the importance of global motion beyond hMT+ (particularly expansion and contraction) and prompts deeper inquiry to understand the various roles involved.

We are also the first to report the isolation of the cerebellum by the optic flow component, rotation, and while this finding needs further elaboration, we suggest that it might reflect a visually mediated component of postural stability.

Acknowledgments

This research was supported by The Wellcome Trust, The Dr. Hadwen Trust, The Lord Dowding Foundation, and The BBSRC Grant No. BBS/B/15562.

Commercial relationships: none.
Corresponding author: Ian E. Holliday.
Email: i.e.holliday@aston.ac.uk.
Address: Aston University, Birmingham B4 7ET, UK.

References

Adjamian, P., Barnes, G. R., Hillebrand, A., Holliday, I. E., Singh, K. D., Furlong, P. L., et al. (2004). Co-registration of magnetoencephalography with magnetic resonance imaging using bite-bar-based fiducials and surface-matching. *Clinical Neurophysiology, 115,* 691–698. [PubMed]

Ahlfors, S. P., Simpson, G. V., Dale, A. M., Belliveau, J. W., Liu, A. K., Korvenoja, A., et al. (1999). Spatiotemporal activity of a cortical network for processing visual motion revealed by MEG and fMRI. *Journal of Neurophysiology, 82,* 2545–2555. [PubMed] [Article]

Albright, T. D. (1989). "Centrifugal directional bias in the middle temporal visual area (Mt) of the Macaque." *Visual Neuroscience, 2,* 177–188. [PubMed]

Allman, J., Miezin, F., & McGuinness, E. (1985). Direction- and velocity-specific responses from beyond the classical receptive field in the middle temporal visual area (MT). *Perception, 14,* 105–126. [PubMed]

Amunts, K., Armstrong, E., Malikovic, A., Hömke, L., Mohlberg, H., Schleicher, A., et al. (2007). Gender-specific left–right asymmetries in human visual cortex. *Journal of Neuroscience, 27,* 1356–1364. [PubMed] [Article]

Anderson, K. C., & Siegel, R. M. (1999). Optic flow selectivity in the anterior superior temporal polysensory area, STPa, of the behaving monkey. *Journal of Neuroscience, 19,* 2681–2692. [PubMed]

Annese, J., Gazzaniga, M. S., & Toga, A. W. (2005). Localization of the human cortical visual area MT based on computer aided histological analysis. *Cerebral Cortex, 15,* 1044–1053. [PubMed] [Article]

Baillet, S., Riera, J. J., Marin, G., Mangin, J. F., Aubert, J., & Garnero, L. (2001). Evaluation of inverse methods and head models for EEG source localization using a human skull phantom. *Physics in Medicine and Biology, 46,* 77–96. [PubMed]

Barraza, J. F., & Grzywacz, N. M. (2005). Parametric decomposition of optic flow by humans. *Vision Research, 45,* 2481–2491. [PubMed]

Barth, D. S., Sutherling, W., Broffman, J., & Beatty, J. (1986). Magnetic localization of a dipolar current source implanted in a sphere and a human cranium. *Electroencephalography and Clinical Neurophysiology, 63,* 260–273. [PubMed]

Beardsley, S. A., & Vaina, L. A. (2005). Psychophysical evidence for a radial motion bias in complex motion discrimination. *Vision Research, 45,* 1569–1586. [PubMed]

Beauchamp, M. S., Cox, R. W., & DeYoe, E. A. (1997). Graded effects of spatial and featural attention on human area MT and associated motion processing areas. *Journal of Neurophysiology, 78,* 516–520. [PubMed] [Article]

Bex, P. J., & Falkenberg, H. K. (2006). Resolution of complex motion detectors in the central and peripheral visual field. *Journal of the Optical Society of America A, Optics, Image Science, and Vision, 23,* 1598–1607. [PubMed]

Bex, P. J., Metha, A. B., & Makous, W. (1998). Psychophysical evidence for a functional hierarchy of motion processing mechanisms. *Journal of the Optical Society of America A, Optics, Image Science, and Vision, 15,* 769–776. [PubMed]

Bex, P. J., Metha, A. B., & Makous, W. (1999). Enhanced motion aftereffect for complex motions. *Vision Research, 39,* 2229–2238. [PubMed]

Bracewell, R. (1986). *The Fourier transform and its applications* (2nd ed.). Reading, NY: McGraw-Hill.

Braddick, O. J., O'Brien, J. M., Wattam-Bell, J., Atkinson, J., Hartley, T., & Turner, R. (2001). Brain areas sensitive to coherent visual motion. *Perception, 30,* 61–72. [PubMed]

Braunstein, M. L. (1968). Motion and texture as sources of slant information. *Journal of Experimental Psychology, 78,* 247–253. [PubMed]

Brookes, M. J., Gibson, A. M., Hall, S. D., Furlong, P. L., Barnes, G. R., Hillebrand, A., et al. (2005). GLM-beamformer method demonstrates stationary field, alpha ERD and gamma ERS co-localisation with fMRI BOLD response in visual cortex. *Neuroimage, 26,* 302–308. [PubMed]

Brosseau-Lachaine, O., Casanova, C., & Faubert, J. (2008). Infant sensitivity to radial optic flow during the first few months of life. *Journal of Vision, 8*(4):5, 1–14, http://journalofvision.org/8/4/5/, doi:10.1167/8.4.5. [PubMed] [Article]

Burr, D. C., & Santoro, L. (2001). Temporal integration of optic flow, measured by contrast and coherence thresholds. *Vision Research, 41,* 1891–1899. [PubMed]

Calow, D., & Lappe, M. (2007). Local statistics of retinal optic flow for self-motion through natural sceneries. *Network: Computation in Neural Systems, 18,* 343–374. [PubMed]

Cinelli, M., Patla, A., & Stuart, B. (2007). Involvement of the head and trunk during gaze reorientation during standing and treadmill walking. *Experimental Brain Research, 181,* 183–191. [PubMed]

Claeys, K. G., Lindsey, D. T., De Schutter, E., & Orban, G. A. (2003). A higher order motion region in human inferior parietal lobule: Evidence from fMRI. *Neuron, 40,* 631–642. [PubMed] [Article]

Cohen, D. (1972). Magnetoencephalography: Detection of brains electrical-activity with a superconducting magnetometer. *Science, 175,* 664–666. [PubMed]

Cook, E. P., & Maunsell, J. H. (2002). Dynamics of neuronal responses in macaque MT and VIP during motion detection. *Nature Neuroscience, 5,* 985–994. [PubMed]

Crouzeix, A., Yvert, B., Bertrand, O., & Pernier, J. (1999). An evaluation of dipole reconstruction accuracy with spherical and realistic head models in MEG. *Clinical Neurophysiology, 110,* 2176–2188. [PubMed]

Crowell, J. A., & Banks, M. S. (1993). Perceiving heading with different retinal regions and types of optic flow. *Perception & Psychophysics, 53,* 325–337. [PubMed]

Dakin, S. C., Mareschal, I., & Bex, P. J. (2005). An oblique effect for local motion: Psychophysics and natural movie statistics. *Journal of Vision, 5*(10):9, 878–887, http://journalofvision.org/5/10/9/, doi:10.1167/5.10.9. [PubMed] [Article]

Domini, F., & Caudek, C. (1999). Perceiving surface slant from deformation of optic flow. *Journal of Experimental Psychology: Human Perception and Performance, 25,* 426–444. [PubMed]

Donner, T. H., Siegel, M., Oostenveld, R., Fries, P., Bauer, M., & Engel, A. K. (2007). Population activity in the human dorsal pathway predicts the accuracy of visual motion detection. *Journal of Neurophysiology, 98,* 345–359. [PubMed] [Article]

Duffy, C. J., & Wurtz, R. H. (1991a). Sensitivity of Mst neurons to optic flow stimuli. I. A continuum of response selectivity to large-field stimuli. *Journal of Neurophysiology, 65,* 1329–1345. [PubMed]

Duffy, C. J., & Wurtz, R. H. (1991b). Sensitivity of Mst neurons to optic flow stimuli. II. Mechanisms of response selectivity revealed by small field stimuli. *Journal of Neurophysiology, 65,* 1346–1359. [PubMed]

Duffy, C. J., & Wurtz, R. H. (1997a). Medial superior temporal area neurons respond to speed patterns in optic flow. *Journal of Neuroscience, 17,* 2839–2851. [PubMed] [Article]

Duffy, C. J., & Wurtz, R. H. (1997b). Planar directional contributions to optic flow responses in MST neurons. *Journal of Neurophysiology, 77,* 782–796. [PubMed] [Article]

Dumoulin, S. O., Bittar, R. G., Kabani, N. J., Baker, C. L., Jr., Le Goualher, G., Bruce Pike, G. B., et al. (2000). A new anatomical landmark for reliable identification of human area V5/MT: A quantitative analysis of sulcal patterning. *Cerebral Cortex, 10,* 454–463. [PubMed] [Article]

Dupont, P., Orban, G. A., De Bruyn, B., Verbruggen, A., & Mortelmans, L. (1994). Many areas in the human brain respond to visual-motion. *Journal of Neurophysiology, 72,* 1420–1424. [PubMed]

Edwards, M., & Badcock, D. R. (1993). Asymmetries in the sensitivity to motion in-depth: A centripetal bias. *Perception, 22,* 1013–1023. [PubMed]

Freeman, T. C., & Fowler, T. A. (2000). Unequal retinal and extra-retinal motion signals produce different perceived slants of moving surfaces. *Vision Research, 40,* 1857–1868. [PubMed]

Freeman, T. C., & Harris, M. G. (1992). Human sensitivity to expanding and rotating motion: Effects of complementary masking and directional structure. *Vision Research, 32,* 81–87. [PubMed]

Freeman, T. C., Harris, M. G., & Meese, T. S. (1996). On the relationship between deformation and perceived surface slant. *Vision Research, 36,* 317–322. [PubMed]

Geesaman, B. J., & Andersen, R. A. (1996). The analysis of complex motion patterns by form/cue invariant MSTd neurons. *Journal of Neuroscience, 16,* 4716–4732. [PubMed] [Article]

Georgeson, M. A., & Harris, M. G. (1978). Apparent foveofugal drift of counterphase gratings. *Perception, 7,* 527–536. [PubMed]

Giachritsis, C. D., & Harris, M. G. (2005). Global versus local image expansion in estimating time-to-contact from complex optic flow. *Perception, 34,* 577–585. [PubMed]

Giaschi, D., Zwicker, A., Young, S. A., & Bjornson, B. (2007). The role of cortical area V5/MT+ in speed-tuned directional anisotropies in global motion perception. *Vision Research, 47,* 887–898. [PubMed]

Gibson, J. J. (1950). *The perception of the visual world.* Boston: Houghton Mifflin.

Gilmore, R. O., Hou, C., Pettet, M. W., & Norcia, A. M. (2007). Development of cortical responses to optic flow. *Visual Neuroscience, 24,* 845–856. [PubMed]

Goossens, J., Dukelow, S. P., Menon, R. S., Vilis, T., & van den Berg, A. V. (2006). Representation of head-centric flow in the human motion complex. *Journal of Neuroscience, 26,* 5616–5627. [PubMed] [Article]

Graziano, M. S., Andersen, R. A., & Snowden, R. J. (1994). Tuning of MST neurons to spiral motions. *Journal of Neuroscience, 14,* 54–67. [PubMed] [Article]

Greenwood, J. A., & Edwards, M. (2007). An oblique effect for transparent-motion detection caused by variation in global-motion direction-tuning bandwidths. *Vision Research, 47,* 1411–1423. [PubMed]

Gurney, K. N., & Wright, M. J. (1996). A model for the spatial integration and differentiation of velocity signals. *Vision Research, 36,* 2939–2955. [PubMed]

Hall, S. D., Barnes, G. R., Hillebrand, A., Furlong, P. L., Singh, K. D., & Holliday, I. E. (2004). Spatio-temporal imaging of cortical desynchronization in migraine visual aura: A magnetoencephalography case study. *Headache, 44,* 204–208. [PubMed]

Hanada, M., & Ejima, Y. (2000). Effects of roll and pitch components in retinal flow on heading judgement. *Vision Research, 40,* 1827–1838. [PubMed]

Händel, B., Lutzenberger, W., Thier, P., & Haarmeier, T. (2007). Opposite dependencies on visual motion coherence in human area MT plus and early visual cortex. *Cerebral Cortex, 17,* 1542–1549. [PubMed] [Article]

Harris, M., Freeman, T., & Hughes, J. (1992). Retinal speed gradients and the perception of surface slant. *Vision Research, 32,* 587–590. [PubMed]

Heuer, H. W., & Britten, K. H. (2004). Optic flow signals in extrastriate area MST: Comparison of perceptual and neuronal sensitivity. *Journal of Neurophysiology, 91,* 1314–1326. [PubMed] [Article]

Heuer, H. W., & Britten, K. H. (2007). Linear responses to Stochastic motion signals in area MST. *Journal of Neurophysiology, 98,* 1115–1124. [PubMed] [Article]

Hillebrand, A., & Barnes, G. R. (2005). Beamformer analysis of MEG data. In *Magnetoencephalography* (vol. 68, pp. 149–+). San Diego, CA: Elsevier Academic Press.

Hillebrand, A., Singh, K. D., Holliday, I. E., Furlong, P. L., & Barnes, G. R. (2005). A new approach to neuroimaging with magnetoencephalography. *Human Brain Mapping, 25,* 199–211. [PubMed]

Holliday, I. E., & Meese, T. S. (2001). A Magneto-encephalographic (MEG) investigation of visual evoked responses to complex motion stimuli. *Neuro-image, 13,* S892–S892.

Holliday, I. E., & Meese, T. S. (2005). Neuromagnetic evoked responses to complex motions are greatest for expansion. *International Journal of Psychophysiol-ogy, 55,* 145–157. [PubMed]

Huk, A. C., Dougherty, R. F., & Heeger, D. J. (2002). Retinotopy and functional subdivision of human areas MT and MST. *Journal of Neuroscience, 22,* 7195–7205. [PubMed] [Article]

Ivins, J., Porrill, J., Frisby, J., & Orban, G. (1999). The 'ecological' probability density function for linear optic flow: Implications for neurophysiology. *Percep-tion, 28,* 17–32. [PubMed]

Jahn, K., Deutschländer, A., Stephan, T., Kalla, R., Wiesmann, M., Strupp, M., et al. (2008). Imaging human supraspinal locomotor centers in brainstem and cerebellum. *Neuroimage, 39,* 786–792. [PubMed]

Jensen, O., & Vanni, S. (2002). A new method to identify multiple sources of oscillatory activity from magneto-encephalographic data. *Neuroimage, 15,* 568–574. [PubMed]

Jokisch, D., Troje, N. F., Koch, B., Schwarz, M., & Daum, I. (2005). Differential involvement of the cerebellum in biological and coherent motion perception. *European Journal of Neuroscience, 21,* 3439–3446. [PubMed]

Kleinschmidt, A., Thilo, K. V., Büchel, C., Gresty, M. A., Bronstein, A. M., & Frackowiak, R. S. (2002). Neural correlates of visual-motion perception as object- or self-motion. *Neuroimage, 16,* 873–882. [PubMed]

Koenderink, J. J. (1986). Optic flow. *Vision Research, 26,* 161–179. [PubMed]

Koenderink, J. J., & van Doorn, A. J. (1975). Invariant properties of the motion parallax field due to the movement of rigid bodies relative to an observer. *Optica Acta, 22,* 773–791.

Koenderink, J. J., & van Doorn, A. J. (1992). "2nd-Order optic flow." *Journal of the Optical Society of America A, Optics, Image Science, and Vision, 9,* 530–538.

Könönen, M., Pääkkönen, A., Pihlajamäki, M., Partanen, K., Karjalainen, P. A., Soimakallio, S., et al. (2003). Visual processing of coherent rotation in the central visual field: An fMRI study. *Perception, 32,* 1247–1257. [PubMed]

Lagae, L., Maes, H., Raiguel, S., Xiao, D. K., & Orban, G. A. (1994). Responses of macaque Sts neurons to optic flow components: A comparison of areas Mt and Mst. *Journal of Neurophysiology, 71,* 1597–1626. [PubMed]

Laird, A. R., Fox, P. M., Price, C. J., Glahn, D. C., Uecker, A. M., Lancaster, J. L., et al. (2005). ALE meta-analysis: Controlling the false discovery rate and performing statistical contrasts. *Human Brain Mapping, 25,* 155–164. [PubMed]

Lancaster, J. L., Tordesillas-Gutiérrez, D., Martinez, M., Salinas, F., Evans, A., Zilles, K., et al. (2007). Bias between MNI and Talairach coordinates analyzed using the ICBM-152 brain template. *Human Brain Mapping, 28,* 1194–1205. [PubMed]

Lancaster, J. L., Woldorff, M. G., Parsons, L. M., Liotti, M., Freitas, C. S., Rainey, L., et al. (2000). Automated Talairach Atlas labels for functional brain mapping. *Human Brain Mapping, 10,* 120–131. [PubMed] [Article]

Lappe, M., Bremmer, F., & van den Berg, A. V. (1999). Perception of self-motion from visual flow. *Trends in Cognitive Sciences, 3,* 329–336. [PubMed]

Lee, D. N., & Aronson, E. (1974). Visual proprioceptive control of standing in human infants. *Perception & Psychophysics, 15,* 529–532.

Lee, D. N. (1980). The optic flow field: The foundation of vision. *Philosophical Transactions of the Royal Society of London B: Biological Sciences, 290,* 169–179. [PubMed]

Liljeström, M., Kujala, J., Jensen, O., & Salmelin, R. (2005). Neuromagnetic localization of rhythmic activity in the human brain: A comparison of three methods. *Neuroimage, 25,* 734–745. [PubMed]

Logan, D. J., & Duffy, C. J. (2006). Cortical area MSTd combines visual cues to represent 3-D self-movement. *Cerebral Cortex, 16,* 1494–1507. [PubMed] [Article]

Longuet-Higgins, H. C., & Prazdny, K. (1980). The Interpretation of a Moving Retinal Image. *Proceedings of the Royal Society of London B: Biological Sciences, 208,* 385–397. [PubMed]

Loomis, J. M., & Nakayama, K. (1973). A velocity analogue of brightness contrast. *Perception, 2,* 425–427. [PubMed]

Malikovic, A., Amunts, K., Schleicher, A., Mohlberg, H., Eickhoff, S. B., Wilms, M., et al. (2007). Cytoarchitectonic analysis of the human extrastriate cortex in the region of V5/MT+: A probabilistic, stereotaxic map of area h0c5. *Cerebral Cortex, 17,* 562–574. [PubMed] [Article]

Martinez-Trujillo, J. C., Cheyne, D., Gaetz, W., Simine, E., & Tsotsos, J. K. (2007). Activation of area MT/V5 and the right inferior parietal cortex during the discrimination of transient direction changes in translational motion. *Cerebral Cortex, 17,* 1733–1739. [PubMed] [Article]

Martinez-Trujillo, J. C., Tsotsos, J. K., Simine, E., Pomplun, M., Wildes, R., Treue, S., et al. (2005). Selectivity for speed gradients in human area MT/V5. *Neuroreport, 16,* 435–438. [PubMed]

Matsumoto, R., Ikeda, A., Nagamine, T., Matsuhashi, M., Ohara, S., Yamamoto, J., et al. (2004). Subregions of human MT complex revealed by comparative MEG and direct electrocorticographic recordings. *Clinical Neurophysiology, 115,* 2056–2065. [PubMed]

Meese, T. S., & Anderson, S. J. (2002). Spiral mechanisms are required to account for summation of complex motion components. *Vision Research, 42,* 1073–1080. [PubMed]

Meese, T. S., & Harris, M. G. (1997). Computation of surface slant from optic flow: Orthogonal components of speed gradient can be combined. *Vision Research, 37,* 2369–2379. [PubMed]

Meese, T. S., & Harris, M. G. (2001a). Broad direction bandwidths for complex motion mechanisms. *Vision Research, 41,* 1901–1914. [PubMed]

Meese, T. S., & Harris, M. G. (2001b). Independent detectors for expansion and rotation, and for orthogonal components of deformation. *Perception, 30,* 1189–1202. [PubMed]

Meese, T. S., Harris, M. G., & Freeman, T. C. (1995). Speed gradients and the perception of surface slant—Analysis is 2-dimensional not one-dimensional. 2879–2888. [PubMed]

Meese, T. S., & Williams, C. B. (2000). Probability summation for multiple patches of luminance modulation. *Vision Research, 40,* 2101–2113. [PubMed]

Morrone, M. C., Burr, D. C., Di Pietro, S., & Stefanelli, M. A. (1999). Cardinal directions for visual optic flow. *Current Biology, 9,* 763–766. [PubMed] [Article]

Morrone, M. C., Burr, D. C., & Vaina, L. M. (1995). Two stages of visual processing for radial and circular motion. *Nature, 376,* 507–509. [PubMed]

Morrone, M. C., Tosetti, M., Montanaro, D., Fiorentini, A., Cioni, G., & Burr, D. C. (2000). A cortical area that responds specifically to optic flow, revealed by fMRI. *Nature Neuroscience, 3,* 1322–1328. [PubMed]

Nakayama, K., & Loomis, J. M. (1974). Optical velocity patterns, velocity-sensitive neurons, and space perception: A hypothesis. *Perception, 3,* 63–80. [PubMed]

Nichols, T. E., & Holmes, A. P. (2001). Nonparametric analysis of PET functional neuroimaging experiments: A primer. *Human Brain Mapping, 15,* 1–25.

Orban, G. A., Claeys, K., Nelissen, K., Smans, R., Sunaert, S., Todd, J. T., et al. (2006). Mapping the parietal cortex of human and non-human primates. *Neuropsychologia, 44,* 2647–2667. [PubMed]

Orban, G. A., Fize, D., Peuskens, H., Denys, K., Nelissen, K., Sunaert, S., et al. (2003). Similarities and differences in motion processing between the human and macaque brain: Evidence from fMRI. *Neuropsychologia, 41,* 1757–1768. [PubMed]

Orban, G. A., Lagae, L., Raiguel, S., Xiao, D., & Maes, H. (1995). The speed tuning of medial superior temporal (MST) cell responses to optic-flow components. *Perception, 24,* 269–285. [PubMed]

Orban, G. A., Van Essen, D., & Vanduffel, W. (2004). Comparative mapping of higher visual areas in monkeys and humans. *Trends in Cognitive Sciences, 8,* 315–324. [PubMed]

Paradis, A. L., Cornilleau-Pérès, V., Droulez, J., Van De Moortele, P. F., Lobel, E., Berthoz, A., et al. (2000). Visual perception of motion and 3-D structure from motion: An fMRI study. *Cerebral Cortex, 10,* 772–783. [PubMed] [Article]

Pfurtscheller, G. (2001). Functional brain imaging based on ERD/ERS. *Vision Research, 41,* 1257–1260. [PubMed]

Prieto, E. A., Barnikol, U. B., Soler, E. P., Dolan, K., Hesselmann, G., Mohlberg, H., et al. (2007). Timing of V1/V2 and V5+ activations during coherent motion of dots: An MEG study. *Neuroimage, 37,* 1384–1395. [PubMed]

Ptito, M., Kupers, R., Faubert, J., & Gjedde, A. (2001). Cortical representation of inward and outward radial motion in man. *Neuroimage, 14,* 1409–1415. [PubMed]

Redlick, F. P., Jenkin, M., & Harris, L. R. (2001). Humans can use optic flow to estimate distance of travel. *Vision Research, 41,* 213–219. [PubMed]

Richards, J. T., Mulavara, A. P., & Bloomberg, J. J. (2004). Postural stability during treadmill locomotion as a function of the visual polarity and rotation of a three-dimensional virtual environment. *Presence: Teleoperators and Virtual Environments, 13,* 371–384.

Rovamo, J., Virsu, V., Laurinen, P., & Hyvärinen, L. (1982). Resolution of gratings oriented along and across meridians in peripheral-vision. *Investigative Ophthalmology & Visual Science, 23,* 666–670. [PubMed] [Article]

Royden, C. S., Banks, M. S., & Crowell, J. A. (1992). The perception of heading during eye-movements. *Nature, 360,* 583–585. [PubMed]

Royden, C. S., & Picone, L. J. (2007). A model for simultaneous computation of heading and depth in the presence of rotations. *Vision Research, 47,* 3025–3040. [PubMed]

Saito, H., Yukie, M., Tanaka, K., Hikosaka, K., Fukada, Y., & Iwai, E. (1986). Integration of direction signals of image motion in the superior temporal sulcus of the macaque monkey. *Journal of Neuroscience, 6,* 145–157. [PubMed] [Article]

Siegel, M., Donner, T. H., Oostenveld, R., Fries, P., & Engel, A. K. (2007). High-frequency activity in human visual cortex is modulated by visual motion strength. *Cerebral Cortex, 17,* 732–741. [PubMed] [Article]

Singh, K. D., Barnes, G. R., & Hillebrand, A. (2003). Group imaging of task-related changes in cortical synchronisation using nonparametric permutation testing. *Neuroimage, 19,* 1589–1601. [PubMed]

Slobounov, S., Wu, T., Hallett, M., Shibasaki, H., Slobounov, E., & Newell, K. (2006). Neural underpinning of postural responses to visual field motion. *Biological Psychology, 72,* 188–197. [PubMed]

Smith, A. T., Wall, M. B., Williams, A. L., & Singh, K. D. (2006). Sensitivity to optic flow in human cortical areas MT and MST. *European Journal of Neuroscience, 23,* 561–569. [PubMed]

Snowden, R. J. (1992). Sensitivity to relative and absolute motion. *Perception, 21,* 563–568. [PubMed]

Snowden, R. J., & Milne, A. B. (1996). The effects of adapting to complex motions: Position invariance and tuning to spiral motions. *Journal of Cognitive Neuroscience, 8,* 435–452.

Snowden, R. J., & Milne, A. B. (1997). Phantom motion aftereffects: Evidence of detectors for the analysis of optic flow. *Current Biology, 7,* 717–722. [PubMed] [Article]

Talairach, J., & Tournoux, P. (1988). *Co-planar stereotaxic atlas of the human brain*. New York: Thieme.

Tanaka, K., Fukada, Y., & Saito, H. A. (1989). Underlying mechanisms of the response specificity of expansion contraction and rotation cells in the dorsal part of the medial superior temporal area of the macaque monkey. *Journal of Neurophysiology, 62,* 642–656. [PubMed]

Tanaka, K., & Saito, H. (1989). Analysis of motion of the visual-field by direction, expansion contraction, and rotation cells clustered in the dorsal part of the medial superior temporal area of the macaque monkey. *Journal of Neurophysiology, 62,* 626–641. [PubMed]

Tootell, R. B., Reppas, J. B., Kwong, K. K., Malach, R., Born, R. T., Brady, T. J., et al. (1995). Functional-analysis of human MT and related visual cortical areas using magnetic resonance imaging. *Journal of Neuroscience, 15,* 3215–3230. [PubMed] [Article]

Treue, S., & Andersen, R. A. (1996). Neural responses to velocity gradients in macaque cortical area MT. *Visual Neuroscience, 13,* 797–804. [PubMed]

Van Essen, D. C., Maunsell, J. H., & Bixby, J. L. (1981). The middle temporal visual area in the Macaque: Myeloarchitecture, connections, functional properties and topographic organization. *Journal of Comparative Neurology, 199,* 293–326. [PubMed]

Vrba, J., & Robinson, S. E. (2001). Signal processing in magnetoencephalography. *Methods, 25,* 249–271. [PubMed]

Wall, M. B., Lingnau, A., Ashida, H., & Smith, A. T. (2008). Selective visual responses to expansion and rotation in the human MT complex revealed by fMRI adaptation. *European Journal of Neuroscience, 27,* 2747–2757. [PubMed]

Wall, M. B., & Smith, A. T. (2008). The representation of egomotion in the human brain. *Current Biology, 18,* 191–194. [PubMed]

Warren, P. A., & Rushton, S. K. (2008). Evidence for flow-parsing in radial flow displays. *Vision Research, 48,* 655–663. [PubMed]

Warren, W. H., Jr., Blackwell, A. W., Kurtz, K. J., Hatsopoulos, N. G., & Kalish, M. L. (1991). On the sufficiency of the velocity-field for perception of heading. *Biological Cybernetics, 65,* 311–320. [PubMed]

Warren, W. H., & Hannon, D. J. (1988). Direction of self-motion is perceived from optical flow. *Nature, 336,* 162–163.

Warren, W. H. Jr., Morris, M. W., & Kalish, M. (1988). Perception of translational heading from optical flow. *Journal of Experimental Psychology: Human Perception and Performance, 14,* 646–660. [PubMed]

Watson, A. B., & Eckert, M. P. (1994). Motion-contrast sensitivity: Visibility of motion gradients of various spatial-frequencies. *Journal of the Optical Society of America A: Optics, Image Science, and Vision, 11,* 496–505.

Watson, J. D., Myers, R., Frackowiak, R. S., Hajnal, J. V., Woods, R. P., Mazziotta, J. C., et al. (1993). Area V5 of the human brain: Evidence from a combined study using positron emission tomography and magnetic resonance imaging. *Cerebral Cortex, 3,* 79–94. [PubMed]

Xiao, D. K., Raiguel, S., Marcar, V., Koenderink, J., & Orban, G. A. (1995). Spatial heterogeneity of inhibitory surrounds in the middle temporal visual area. *Proceedings of the National Academy of Sciences of the United States of America, 92,* 11303–11306. [PubMed] [Article]

Zanker, J. M., & Zeil, J. (2005). Optic flow in natural environments: A downunder perspective. *Perception, 34,* 252–252.

Zhong, H., Cornilleau-Pérès, V., Cheong, L. F., Yeow, G. M., & Droulez, J. (2006). The visual perception of plane tilt from motion in small field and large field: Psychophysics and theory. *Vision Research, 46,* 3494–3513. [PubMed]